Manuscript Details

Manuscript number	MICRES_2019_1272_R1
Title	The rhizosphere signature on the cell motility, biofilm formation and secondary metabolite production of a plant-associated Lysobacter strain
Article type	Research Paper

Abstract

Lysobacter spp. are common bacterial inhabitants of the rhizosphere of diverse plant species. However, the impact of the rhizosphere conditions on their physiology is still relatively understudied. To provide clues on the behaviour of Lysobacter spp. in this ecological niche, we investigated the physiology of L. capsici AZ78 (AZ78), a biocontrol strain isolated from tobacco rhizosphere, on a common synthetic growth medium (LBA) and on a growth medium containing components of the plant rhizosphere (RMA). The presence of a halo surrounding the AZ78 colony on RMA was a first visible effect related to differences in growth medium composition and it corresponded to the formation of a large outer ring. The lower quantity of nutrients available in RMA as compared with LBA was associated to a higher expression of a gene encoding cAMP-receptor-like protein (Clp), responsible for cell motility and biofilm formation regulation. AZ78 cells on RMA were motile, equipped with cell surface appendages and organised in small groups embedded in a dense layer of fibrils. Metabolic profiling by mass spectrometry imaging revealed increased diversity of analytes produced by AZ78 on RMA as compared with LBA. In particular, putative cyclic lipodepsipeptides, polycyclic tetramate macrolactams, cyclic macrolactams and other putative secondary metabolites with antibiotic activity were identified. Overall, the results obtained in this study shed a light on AZ78 potential to thrive in the rhizosphere by its ability to move, form biofilm and release secondary metabolites.

Keywords	Rhizosphere; Lysobacter; biofilm; cell motility; secondary metabolites; mass spectrometric imaging

Corresponding Author	Gerardo Puopolo
Corresponding Author's Institution	Fondazione Edmund Mach
Order of Authors	Francesca Brescia, Martina Marchetti-Deschmann, Rita Musetti, Michele Perazzolli, Ilaria Pertot, Gerardo Puopolo
Suggested reviewers	Joeke Postma, Irina Kudryakova, Klaus Dreisewerd

Submission Files Included in this PDF

File Name [File Type]

Covering Letter_031219.doc [Cover Letter]

Response to reviewers_090120.docx [Response to Reviewers]

Highlights_031219.docx [Highlights]

Revised Draft_090120.docx [Manuscript File]

Figure 1_031219.pptx [Figure]

Figure 2_031219.pptx [Figure]

Figure 3_031219.pptx [Figure]

Figure 4_031219.pptx [Figure]

Figure A1_031219.pptx [Figure]

Figure A2_031219.pptx [Figure]

Figure A3_031219.pptx [Figure]

Declaration_090120.docx [Author Statement]

Submission Files Not Included in this PDF

File Name [File Type]

Animation A1A_031219.mp4 [Video Still]

Animation A1B_031219.mp4 [Video Still]

To view all the submission files, including those not included in the PDF, click on the manuscript title on your EVISE Homepage, then click 'Download zip file'.

Dear Editor in Chief,

We would be very grateful if you could consider this manuscript entitled **"The rhizosphere signature on the cell motility, biofilm formation and secondary metabolite production of a plant-associated *Lysobacter* strain"** for publication in Microbiological Research.

We feel that the manuscript fits in well with the aims and scope of the journal, as it provides insights on the impact of the rhizosphere on the behaviour of a bacterial strain belonging to *Lysobacter*, a bacterial genus including species associated to the rhizosphere of several plant species.

In this work, we used *Lysobacter capsici* AZ78, an effective biocontrol agent isolated from tobacco rhizosphere, as a model strain and we applied molecular, microscopic and analytical techniques to determine the role played by rhizosphere on its physiology.

Results clearly showed that *L. capsici* AZ78 cell growth was slower when it was grown on a growth medium containing components of plant rhizosphere compared to a synthetic growth medium. The slow growth of *L. capsici* AZ78 cell was associated to the up-regulation of *clp* encoding a cAMP-receptor-like protein, a master regulator that responds to nutrient limitation. According to the role played by Clp in the physiology of *Xanthomonadaceae* members, the growth medium containing components of plant rhizosphere positively modulated the ability of *L. capsici* AZ78 cells to move on solid surfaces, form biofilm and produce bioactive secondary metabolites.

We feel confident that the results obtained in this work will be useful for a more accurate characterisation of bacterial strains belonging to other plant-associated *Lysobacter* species. Moreover, the results may pave the way to future studies aimed at better understanding the ecological role played by *Lysobacter* spp. in agricultural soils and the plant rhizosphere.

Best regards,

Gerardo Puopolo

Dear Editor and Reviewers,

we are very honoured to have received a positive feedback from your Journal. We take this occasion to thank the Reviewer 1 for her/his constructive revision.
We have revised our manuscript according to reviewer's comments and the changes are highlighted in the revised version of our manuscript. Moreover, se also edited typing errors found in the main text and the references were double checked. We report our revisions below.
We do hope that the revised version of the manuscript may be accepted.
Best regards,
Gerardo Puopolo

Reviewer 1

1. It is possible to create table in which will indicate all *m/z* of compounds determined by MALDI-TOF-MSI and their preliminary annotation. It can help unload chapter 3.2 in Results.

> We agree with the Reviewer comment and two supplementary tables (Table A.1, A.2) have been included in the revised version of the manuscript. According to the comment, the *m/z* of analytes produced by *Lysobacter capsici* AZ78 cells grown on RMA (Table A.1) and LBA (Table A.2) identified through MALDI-TOF-MSI and their possible matching compounds have been reported in these tables.

2. It is better change sentence « Many of these bioactive secondary metabolites are encoded by polyketide synthase (PKS) gene clusters» on polyketide synthase (PKS) gene clusters is responsible for the biosynthesis of many of these bioactive secondary metabolites in lines 103-104.

> The sentence has been changed accordingly.

3. Decoding of abbreviations MALDI-TOF-MSI and TEM were in lines 114-115, so subsequent mention of them could be as abbreviations (eg, lines 212, 245). Same for *Lysobacter*: *L. capsici* instead *Lysobacter capsici* (lines 119, 292 and others).

> We thank the reviewer for the comment and the abbreviations have been carefully checked in the revised version of the manuscript. However, we have not used the abbreviation for *Lysobacter capsici* in the paragraph titles.

4. Lines 320-321: RM instead SR. Figure 4 instead Figure 5 (line 849).

> The main text was edited according to these comments.

Highlights

- Behaviour of plant beneficial *Lysobacter* spp. in the rhizosphere is understudied
- A growth medium mimicking rhizosphere conditions was designed
- Rhizosphere conditions affected colony morphology and cell motility
- Expression of *clp* and biofilm formation were positively influenced
- A higher production of bioactive metabolites was observed in rhizosphere conditions

The rhizosphere signature on the cell motility, biofilm formation and secondary metabolite production of a plant-associated *Lysobacter* strain

Francesca Brescia[ab], Martina Marchetti-Deschmann[c], Rita Musetti[d], Michele Perazzolli[ae], Ilaria Pertot[ae], Gerardo Puopolo[ae]*

[a]Department of Sustainable Agro-ecosystems and Bioresources, Research and Innovation Centre, Fondazione Edmund Mach, Via E. Mach 1, 38010 San Michele all'Adige, Italy

[b]PhD school in Agricultural Science and Biotechnology, Department of Agricultural, Food, Environmental and Animal Sciences, University of Udine, Udine, Italy

[c]Institute of Chemical Technologies and Analytics, TU Wien (Vienna University of Technology), Vienna, 1060, Austria

[d]Department of Agricultural, Food, Environmental and Animal Sciences, University of Udine, Udine, 33100, Italy

[e]Center Agriculture Food Environment (C3A), University of Trento, Via E. Mach 1, 38010 San Michele all'Adige, Italy

*Corresponding author: Gerardo Puopolo; E-mail address: gerardo.puopolo@unitn.it, Postal address: Department of Sustainable Agro-ecosystems and Bioresources, Research and Innovation Centre, Fondazione Edmund Mach, Via E. Mach 1, 38010 San Michele all'Adige, Italy

Abstract

Lysobacter spp. are common bacterial inhabitants of the rhizosphere of diverse plant species. However, the impact of the rhizosphere conditions on their physiology is still relatively understudied. To provide clues on the behaviour of *Lysobacter* spp. in this ecological niche, we investigated the physiology of *L. capsici* AZ78 (AZ78), a biocontrol strain isolated from tobacco rhizosphere, on a common synthetic growth medium (LBA) and on a growth medium containing components of the plant rhizosphere (RMA). The presence of a halo surrounding the AZ78 colony on RMA was a first visible effect related to differences in growth medium composition and it corresponded to the formation of a large outer ring. The lower quantity of nutrients available in RMA as compared with LBA was associated to a higher expression of a gene encoding cAMP-

receptor-like protein (Clp), responsible for cell motility and biofilm formation regulation. AZ78 cells on RMA were motile, equipped with cell surface appendages and organised in small groups embedded in a dense layer of fibrils. Metabolic profiling by mass spectrometry imaging revealed increased diversity of analytes produced by AZ78 on RMA as compared with LBA. In particular, putative cyclic lipodepsipeptides, polycyclic tetramate macrolactams, cyclic macrolactams and other putative secondary metabolites with antibiotic activity were identified. Overall, the results obtained in this study shed a light on AZ78 potential to thrive in the rhizosphere by its ability to move, form biofilm and release secondary metabolites.

Abbreviations

LBA, Luria-Bertani Agar; RMA, Rhizosphere-Mimicking Agar; Clp, cAMP-receptor-like protein; HSAF, heat stable antifungal factor; MALDI-TOF-MSI, Matrix Assisted Laser Desorption Ionisation Time of Flight Mass Spectrometric Imaging; TEM, Transmission Electron Microscopy; cfu, colony forming units; TSA, Tryptic Soy Agar; qRT-PCR, quantitative real-time Polymerase Chain Reaction; Ct, cycle threshold; RQ, relative quantities; OD, optical density; SBF, specific biofilm formation; 2,5-DHB, 2,5-dihydroxybenzoic acid; α-CHCA, α-cyano-4-hydroxy-cinnamic acid; CC, centre core; OR, outer ring; GM, growth medium; ANOVA, analysis of variance; CRP, cAMP receptor protein.

Keywords

Rhizosphere, *Lysobacter*, biofilm, cell motility, secondary metabolites, mass spectrometric imaging

Declaration of interests

The authors declare that they have no known competing financial interests or personal relationships that could have appeared to influence the work reported in this paper

1. Introduction

In the rhizosphere, plant roots release organic matter, including root exudates, in an important and metabolically expensive process called rhizodeposition (Walker et al., 2003). It was estimated that young plants can invest in root exudates about 30-40% of their fixed carbon (Lynch and Whipps, 1990). Root exudates mainly encompass carbon-based compounds, such as amino acids, organic acids, sugars, secondary metabolites and high-molecular weight compounds like mucilage and proteins (Uren, 2007). The dialogue between plants and microbial community based on

rhizodeposition is continuous and microbial communities change during plant development according to the chemical composition of root exudates (Zhalnina et al., 2018). As these compounds are an easily available carbon source for soil microbes (van Hees et al., 2005), plants may improve their own fitness by actively selecting beneficial bacteria through rhizodeposition (Doornbos et al., 2012; Kobayashi et al., 2013). The capacity of plants to modify the microflora inhabiting the rhizosphere was demonstrated by adding root exudates or synthetic root exudates to solidified media or to formulated synthetic soils (Baudoin et al., 2003; Downie et al., 2012; Grayston et al., 1998), indicating that structural manipulation of rhizobacterial communities can be mediated by root exudates. The same approach was followed also to determine how the rhizosphere conditions may impact the behaviour of plant beneficial bacteria. In this way, it was shown that compounds exuded in the rhizosphere may actively modulate bacterial physiological traits such as formation of biofilm and biosynthesis of secondary metabolites (Debois et al., 2015; Kamilova et al., 2006; Nihorimbere et al., 2012). Therefore, a complex molecular crosstalk takes place at the soil-root interface. For instance, when beneficial bacteria sense the presence of the plant, they induce the systemic resistance of the plant starting the production of secondary metabolites (Debois et al., 2015).

Among the common inhabitants of plant rhizosphere, it was recently shown that *Lysobacter* spp. was part of the core microbiome of the rhizosphere of switchgrass (*Panicum virgatum* L.) plants collected from different soils and environments (Rodrigues et al., 2018). Regarding crop plants, type strains of *Lysobacter* spp. were isolated from the rhizosphere of pepper (*Capsicum annuum* L.), rice (*Oryza sativa* L.) and tomato (*Solanum lycopersicum* L.) plants, providing another proof of *Lysobacter* spp. as common inhabitants of plant rhizospheres (Aslam et al., 2009; Kim et al., 2017; Park et al., 2008). Notably, the presence of *Lysobacter* members in agricultural soils was often found in correlation with the suppressiveness of these soils against plant pathogenic

84 microorganisms such as *Ralstonia solanacearum*, *Rhizoctonia solani* and *Streptomyces* spp.
85 (Postma et al., 2010; Rosenzweig et al., 2012; Wang et al., 2017).

86 The involvement of *Lysobacter* spp. in the active control of plant pathogens is sustained by their
87 capacity to prey upon other microorganisms through a wolf-pack behaviour (Seccareccia et al.,
88 2015) and to produce a vast array of lytic enzymes and bioactive secondary metabolites (Puopolo et
89 al., 2018). *Lysobacter* biocontrol strains are characterised by the ability to produce toxic compounds
90 belonging to the polycyclic tetramate macrolactams family against *Peronosporomycetes,* as in the
91 case of Xanthobaccins A, B and C produced by *L. capsici* SB-K88 (Islam et al., 2005; Nakayama et
92 al., 1999; Puopolo et al., 2018). Remaining in this family of bioactive secondary metabolites,
93 particular interest was given to the dihydromalthophilin, also called heat stable antifungal factor
94 (HSAF) produced by the biocontrol strain *L. enzymogenes* C3 (Yu et al., 2007), since it was
95 involved in the control of plant pathogenic fungi and nematodes (Li et al., 2008; Yuen et al., 2018).
96 The toxicity of dihydromalthophilin/HSAF was related to its ability to trigger the production of
97 reactive oxygen species and its negative impact on the sphingolipid biosynthesis and tricarboxylic
98 acid cycle (Amin et al., 2015; Ding et al., 2016; He et al., 2018; Li et al., 2009). Interestingly, the
99 same bacterial strain was also able to produce other three polycyclic tetramate macrolactams,
100 namely alteramide A, lysobacteramide A and B that, besides antifungal activity, showed activity
101 against human carcinoma also (Xu et al., 2015). Other bioactive secondary metabolites produced by
102 *Lysobacter* biocontrol strains received particular attention from sectors other than agriculture as in
103 the case of the cyclic lipodepsipeptides WAP-8294A produced by *L. enzymogenes* OH11 toxic
104 against human pathogenic Gram-positive bacteria (Zhang et al., 2011). Polyketide synthase (PKS)
105 gene clusters are responsible for the biosynthesis of many of these bioactive secondary metabolites
106 (Xie et al., 2012). Polyketides are natural products structurally diverse as, once produced, they
107 undergo post-PKS modifications (Pfeifer and Khosla, 2001). However, little is known on how
108 rhizosphere conditions might influence the physiological traits of *Lysobacter* plant beneficial strains

and the biosynthesis of secondary metabolites. To shed a light on aspects of rhizosphere colonization and secondary metabolite production, we formulated a culture medium containing components present in the plant rhizosphere and we evaluated its impact on the physiological traits of *L. capsici* AZ78 (AZ78), a biocontrol agent isolated from tobacco rhizosphere (Puopolo et al., 2014a). Particular attention was given to the capacity of this strain to move on solid surfaces, form biofilm and to release bioactive secondary metabolites. The AZ78 metabolic profile was investigated using Matrix Assisted Laser Desorption Ionisation Time of Flight Mass Spectrometric Imaging (MALDI-TOF-MSI), while Transmission Electron Microscopy (TEM) and phase-contrast microscopy were used to visualise motility appendages and the AZ78 macrocolony structure.

2. Materials and methods

2.1 Maintenance and preparation of Lysobacter capsici *AZ78 cell suspension*

AZ78 was stored at length in glycerol 40% at -80°C and routinely grown at 27°C on Luria–Bertani Agar [LBA; LB broth (Sigma Chemical-St. Louis, MO,USA, Tryptone 10 g/l, Yeast Extract 5 g/l, NaCl 10 g/l), Agar Technical No.2 16 g/l (Oxoid-Columbia, MD, USA)] in Petri dishes (90 mm diameter). To prepare cell suspension, AZ78 cells were picked from LBA dishes after 48 h incubation at 27°C using sterile 10 µl loops and suspended in 1 ml sterile saline solution (0.85% NaCl w/v) contained into sterile 2 ml microcentrifuge tubes. The AZ78 cell suspension was centrifuged (13,000 rpm, 1 min), supernatant was discarded and the pellet was suspended in 1 ml sterile saline solution. These steps were repeated twice to remove any trace of nutrients from LBA and secondary metabolites released during AZ78 growth. Finally, AZ78 pelleted cells were suspended into sterile saline solution, adjusted to a final concentration of 1×10^9 colony forming units per volume unit (cfu/ml) and used in all experiments.

133 *2.2 Rhizosphere-Mimicking growth medium*

134 The growth medium named Rhizosphere-Mimicking Agar (RMA) was prepared simulating the
135 amount of carbon released by plants in the rhizosphere soil in one day according to Chen et al.
136 (2006) and Jones et al. (2009). The ingredients included synthetic root exudates, recalcitrant organic
137 carbon sources and salts (Table 1; Baudoin et al., 2003). RMA ingredient concentrations were
138 estimated taking into account that plant tissue residues in soil are related to their decomposition rate
139 (Chen et al., 2001). The pH was adjusted to 6.5 and Agar Technical No. 2 (Oxoid) was added (16
140 g/l). To avoid caramelization, sugars were filter-sterilised (0.2 µm Sartorius, Göttingen, Germany)
141 and added after autoclaving.

142

143 *2.3 Cell growth*

144 Five µl of AZ78 cell suspension were spot-inoculated on LBA and RMA Petri dishes (50 mm
145 diameter) and incubated at 25°C. The growth of AZ78 on LBA and RMA was monitored at 12, 24
146 and 36 h by capturing digital images of AZ78 macrocolonies using Bio-Rad Quantity One software
147 implemented in a Bio-Rad Geldoc system (Bio-Rad Laboratories, Inc., Hercules, California,
148 U.S.A.). Subsequently, the AZ78 macrocolony area was measured using Fiji software (ImageJ1.50i;
149 Schneider et al., 2012). To determine the quantity of AZ78 viable cells residing in the macrocolony
150 area, plugs (5 mm diameter) were sampled from each macrocolony and transferred into sterile 2 ml
151 microcentrifuge tubes containing 1 ml of sterile saline solution amended with Tween 20 (0.1% v/v).
152 A sonication step was used to dissolve cell aggregates using three cycles of gentle sonication: 15 s
153 at 15% of the power of the device [Branson sonifier 250-450 (Ultrasonics Corporation, Danbury,
154 Connecticut, USA)] alternated to 10 s of pause. The resulting solution was serially diluted and
155 plated on Tryptic Soy Agar 1/10 [TS broth (Sigma); Agar Technical No.2 (Oxoid) 16 g/l (w/v)], cfu
156 were counted 48 h after incubation at 25°C and the cell concentration was expressed as the $\log_{10}$

(cfu)/macrocolony. Three replicates (Petri dishes) for each time-point were used and the experiment was carried out twice.

2.4 Total RNA extraction and gene expression analysis

Five µl of AZ78 cell suspension were spot-inoculated on LBA and RMA (3 ml) contained in Petri dishes (50 mm diameter). RNA was extracted after 36 h incubation at 25°C from macrocolonies developed on LBA and RMA according to the following procedure. Agar plugs (5 mm diameter) were collected in aluminium paper and instantly frozen in liquid nitrogen. The frozen plugs were placed in pre-frozen steel jars containing sterile beads and processed at 25 Hz for 1 min using a mixer mill disruptor (MM200, Retsch, Haan, Germany). The resulting powder was transferred into sterile 2 ml RNAse-free microcentrifuge tubes placing up to 100 mg of powder each. To lyse the AZ78 cell wall, 0.3 ml of lysis buffer (30 mM Tris, 30 mM EDTA, 10 mg/ml lysozyme, pH 6.2) were added to each microcentrifuge tube, vortexed vigorously and incubated at 37°C with constant shaking (1,000 rpm) for 30 min (Villa-Rodríguez et al., 2018). RNA was extracted using Spectrum™ Plant Total RNA Kit (Sigma-Aldrich) according to manufacturer's instructions. The extracted RNA was run in a 1% agarose gel to assess the integrity and quantified using Qubit® Fluorimetric Quantitation (Invitrogen, Life Technologies, Waltham, MA) with Qubit RNA BR assay (Invitrogen, Life Technologies). RNA was long term stored at -80°C. To process similar quantities of AZ78 cells, three replicates respectively made by five and 40 Petri dishes for LBA and RMA were used for each treatment and the experiments were carried out twice.

To carry out quantitative real-time PCR (qRT-PCR), first-strand cDNA was synthesised from 900 ng of purified total RNA with the SuperScript III Reverse Transcriptase RT kit (Thermo Fisher Scientific, Invitrogen, Waltham, Massachusetts, U.S.A.) with random hexamers, according to the manufacturer's instructions. qRT-PCR were carried out to monitor the expression level of the gene

AZ78_4111 encoding a cAMP-receptor-like protein (Clp), responsible for cell motility and biofilm formation, using previously designed primers (clpF: ACTCGGCCTATTCATCGAAA, clpR: GTCAGCAGCAGGTCGTACAG; Tomada et al., 2016).

The qRT-PCR reactions were carried out with LightCycler 480 (Roche Diagnostics, Mannheim, Germany) and Platinum SYBR Green qPCR SuperMix-UDG (Thermo Fisher Scientific, Invitrogen) and they consisted of 60 amplification cycles (95°C for 15 s and 60°C for 45 s) and melting curve analysis. LightCycler 480 SV1.5.0 software (Roche Diagnostics) was used to extract the cycle threshold (Ct) values using the second derivative calculation. LinRegPCR 11.1 software (Ruijter et al., 2009) was used to calculate the reaction efficiency. The relative quantities (RQ) were calculated according to the formula:

$$RQ = Eff^{(Ct-Ct^*)}$$

where Ct is the threshold cycle and Ct* is the average Ct of all the conditions analysed (Hellemans et al., 2007). To calculate the normalised relative quantities (NRQ) the RQ values of *AZ78_4111* were divided by the RQ of the housekeeping gene *AZ78_1089* encoding RecA using the previously designed primers (recAF: GAGCCAGATCGACAAGCAAT, recAR :GGACCGTAGATCTCGACCAC; Tomada et al., 2016). For each treatment, three replicates were used and qRT-PCR reactions were carried out for two independent experiments.

2.5 Cell motility

The impact of LBA and RMA on AZ78 cell motility was assessed according to Chen et al. (2018). Briefly, a sterilised glass slide was placed into a Petri dish (90 mm diameter) and 14 ml of LBA and/or RMA were poured on the top. Once solidified, the agar medium in excess was removed with a sterile scalpel and discarded. To create a thin inoculation line, the edge of a sterilised coverslip was dropped into an AZ78 cell suspension and then gently pressed onto the surface of each

205 medium. After 36 h incubation at 25°C in a wet chamber, the glass slides were observed using a
206 phase-contrast microscope (Nikon Eclipse 80i, Tokyo, Japan) under 20X and 100X magnification.
207 Pictures were taken with a digital camera (Nikon DS-Fi1) connected to the microscope, stop-motion
208 animations were made taking 10 pictures in 100 s at regular intervals and reproduced with an
209 interval of 0.5 s, while videos were recorded using a Olympus OMD EM-10 camera (Olympus,
210 Tokyo, Japan) connected to the microscope. Three replicates (glass slides) for each treatment were
211 prepared and the experiment was carried out twice.

212

213 *2.6 Transmission Electron Microscopy (TEM)*

214 AZ78 was grown on LBA and RMA for 36 h at 25°C. To obtain a similar quantity of cells, AZ78
215 cells were collected with a sterile loop from the borders of the macrocolony developed on 40 RMA
216 dishes (50 mm diameter) and on five LBA dishes (50 mm diameter) and suspended in 1 ml of sterile
217 distilled water contained in sterile 2 ml microcentrifuge tubes. Drops (50 µl) of the cell suspension
218 were adsorbed to TEM carbon-formvar coated nickel grids for 10 min, at room temperature. The
219 bacterial cells were then stained 10 min with UAR-EMS (uranyl acetate replacement stain)
220 (Electron Microscopy Sciences, Fort Washington, PA, USA), and observed under a PHILIPS CM
221 10 (FEI, Eindhoven, The Netherlands) transmission electron microscope (Cowles and Gitai, 2010),
222 operated at 80 kV, and equipped with a Megaview G3 CCD camera (EMSIS GmbH, Münster,
223 Germany). Three replicates for each treatment were used and the experiment was carried out twice.

224

225 *2.7 Biofilm production*

226 AZ78 was evaluated for its ability to form biofilm on polystyrene microtiter plates according to
227 Puopolo et al. (2014a). Briefly, 1.5 µl of AZ78 cell suspension was inoculated into 150 µl of sterile

228 LB broth (LB) and Rhizosphere Mimicking broth (RM) contained in 96-well polystyrene plates.
229 Wells containing uninoculated LB and RM were used as untreated samples. Plates were incubated
230 for 36 h at 25°C without shaking and cell densities were determined by scoring the absorbance at
231 optical density (OD) 600 nm ($A_{OD600nm}$). Unattached cells were removed by inverting the plate and
232 tapping it vigorously onto absorbent paper. The AZ78 cells adhering to the wells were fixed for 20
233 min at 50°C and then stained for one min adding 150 µl of crystal violet solution (0.1% w/v in
234 sterile distilled water) per well. Excess stain was removed by inverting the plate, then washing it
235 twice with distilled water (250 µl per well). Adherent cells were decolorized with an
236 acetone/ethanol (20%/80%) solution (200 µl per well) for five min to release the dye into the
237 solution. A volume of 100 µl was transferred from each well to another 96-well polystyrene plate
238 and the amount of dye (proportional to the density of adherent cells) was quantified by scoring the
239 absorbance at OD 540 nm ($A_{OD540nm}$). To determine the specific biofilm formation value (SBF) the
240 following formula was applied:

241 $SBF = (A_{OD540nm}X - A_{OD540nm}C) / (A_{OD600nm}X - A_{OD600nm}C)$

242 where X indicated the treated samples whereas C indicated the untreated samples. For each
243 treatment, ten replicates (wells) were used and the experiment was carried out twice.

244

245 *2.8 Matrix Assisted Laser Desorption/Ionisation Time of Flight Mass Spectrometric Imaging*
246 *(MALDI-TOF-MSI)*

247 AZ78 cells were spot-inoculated on 1 mm thick growth medium layer (LBA and/or RMA) poured
248 onto sterile glass slides. To get reproducible conditions an even and smooth surface is of importance
249 for MALDI-TOF-MSI. For this, we further developed our recently published microassay
250 (Holzlechner et al., 2016) and used two sterile glass slides which were hold in place in a distance of
251 exactly 1 mm by sterile spacers. This construct was placed in a sterile Petri dish (90 mm diameter)

252 and 13 ml of growth medium were poured in the Petri dish filling also the gap between the slides
253 giving an area of 5.5 × 2.5 cm. Once solidified, the medium in excess was cut and discarded and the
254 glass slide on the top and the spacers were gently removed. Lastly, five µl of AZ78 cell suspension
255 were spot inoculated on the growth medium layer adhering to the glass slides. An area of 25 mm^2 of
256 growth medium was kept apart from the inoculated medium in order to identify the mass
257 spectrometric signals (*m/z* values) belonging to the growth medium (blank).

258 Once inoculated, the glass slides were incubated at 25°C for 36 h and, subsequently, samples were
259 dried in a desiccator under vacuum overnight at room temperature. Afterwards, a photograph was
260 taken using a glass slides scanner and 0.15-0.20 mg of a 1:1 mixture of 2,5-dihydroxybenzoic acid
261 (2,5-DHB) and α-cyano-4-hydroxy-cinnamic acid (α-CHCA) were sublimed per cm^2 onto the
262 sample using a home-built instrumentation. A subsequent recrystallization step at 86°C for 1 min
263 using 1% acetic acid in water ensured analyte incorporation (Yang and Caprioli, 2011). MALDI-
264 TOF-MSI experiments were then immediately performed on a Synapt G2 HDMS (Waters, Milford,
265 Massachusetts, United States) in positive linear mode, with 150 × 75 µm laser step, the laser energy
266 was set to 250 a.u., 1000 Hz of firing rate, 1 scan per pixel and a mass range of 20–4000 Da. For
267 accurate mass measurements, the instrument was calibrated before each run using red phosphorous.
268 Data of three biological replicates of the microassay per treatment (growth medium) were analysed
269 using Datacube Explorer (Klinkert et al., 2014), MSiReader (Robichaud et al., 2013), and
270 MassLynx (Waters). For tentative assignment of analytes to measure signals, accurate *m/z* values (±
271 0.002 Da) extracted from the profile mass spectra were submitted to "The Metabolomics
272 Workbench" (http://www.metabolomicsworkbench.org/, 2019) and searched in literature. To carry
273 out a presence/absence analysis, *m/z* values that were not present in the blank were searched in the
274 centre core (CC), the outer ring (OR) of the AZ78 macrocolony and in a sector of growth medium
275 adjacent to the OR of the AZ78 macrocolony (GM).

276

277 *2.9 Genome mining*

278 An antiSMASH 5.0.0 analysis (Blin et al., 2019; https://antismash.secondarymetabolites.org) was
279 used to find gene clusters potentially involved in the biosynthesis of bioactive secondary
280 metabolites in AZ78 genome (JAJA02000000.2; Puopolo et al., 2016). The detection strictness of
281 the analysis was relaxed and the extra features KnownClusterBlast, ClusterBlast, ActiveSiteFinder,
282 Cluster Pfam analysis and Pfam-based GO term annotation were selected.

283

284 *2.10 Statistical analysis*

285 The statistical analysis was performed using R package (https://www.r-project.org/). The repetitions
286 of the experiments were tested for significant differences with a two-way analysis of variance
287 (ANOVA). In absence of significant differences, the experiments were pooled and data were
288 analysed using one-way ANOVA. Mean comparisons were carried out using Student's *T*-test
289 (α=0.05).

290

291 **3. Results**

292 *3.1 Growth medium modulates* Lysobacter capsici *AZ78 cell growth and the expression of the*
293 *master regulator* clp

294 The appearance of AZ78 macrocolony changed according to the growth medium. It was creamy and
295 yellowish on LBA (Figure 1A), while it was whitish-transparent on RMA (Figure 1B). Moreover,
296 the macrocolony was surrounded by a halo that reached the maximum area after 36 h growth
297 exclusively on RMA (Figure 1B). The different appearance of AZ78 macrocolony was associated to
298 differences in the AZ78 cell growth. At each time point, the number of AZ78 viable cells residing
299 in the macrocolony was two orders of magnitude lower on RMA than on LBA (Figure 1C). These

differences were associated to a higher *clp* expression on RMA (3.11 ± 0.25; mean ± standard error) than LBA (0.46 ± 0.01; Figure A1).

3.2 Morphology of Lysobacter capsici *AZ78 macrocolonies and cell motility are affected by growth medium*

AZ78 macrocolonies developed on LBA showed a well-defined and compact growth front with cells tightly disposed on the surface of the medium (Figure 2A). On LBA, a centre core (CC) composed by multiple layers of cells and a mono-layer outer ring (OR) were identified (Figure 2B). A CC constituted by multiple cell layers was also observed on RMA (Figure 2C). However, the mono-layer OR observed on RMA was more extended compared to LBA and the AZ78 cells were disposed in small groups packed along the same axis (Figure 2D). Moreover, AZ78 cells moved on RMA surface, while no cell movement was observed on LBA surface (Animation A1A, B).

TEM analysis revealed that many of the AZ78 cells grown on LBA were in division and were surrounded by heterogeneous biomaterials such as membrane vesicles, long fibrils and cellular detritus (Figure 3A, B, C). Compared to RMA, AZ78 cells grown on LBA were slightly bigger and their cytoplasm presented nucleoid-like areas with low electron density (Figure 3A, C). When grown on RMA, AZ78 cells were tightly packed along the same axis in small groups, surrounded by fibrils and by electron-dense granules, probably part of the extracellular polymeric substance (Figure 3D, E). Polar fimbriae were visible in some AZ78 cells grown on RMA only (Figure 3F).

These differences on the cell morphology due to the growth medium were also reflected in the different capacity of AZ78 cells to form biofilm in LB and RM (Figure A2). The SBF values reached by AZ78 in RM (0.55 ± 0.09) were five time higher than those reached in LB (0.11 ± 0.01).

3.3 The growth medium impacts Lysobacter capsici *AZ78 metabolic profile and analyte spatial distribution*

In general, the comparison of the metabolic profiles of AZ78 macrocolonies originated on the two growth media revealed a higher quantity number of biologically relevant signals on RMA compared to LBA (Figure 4A; Table A.1, A.2); whereas the ion intensities in RMA were lower than in LBA. Moreover, almost no spatial differentiation was observed for CC and OR in LBA. In contrast, the OR was clearly distinguishable from the rest of the AZ78 macrocolony in MALDI-TOF-MSI images on RMA (Figure 4A, B). On RMA, no biologically relevant signals were found in the GM region, but 35 signals were detected inside the OR and CC regions (Figure 4A; Table A.1). Among the latter, 31 *m/z* values were shared by OR and CC regions while four signals were found in the OR region only. In particular, *m/z* 498.973, tentatively assigned to be thiamine pyrophosphate based on accurate mass measurements, was exclusively found in the OR region of RMA and was not present in the three regions of AZ78 macrocolony on LBA (Figure 4A).

The high number of signals found in the CC and OR of AZ78 macrocolonies developed on RMA was characterised by a robust presence of analytes (*m/z* 523.455, 750.467, 762.459, 764.433, 778.430, 806.469, 1421.856, 1423.823) that might match compounds belonging to the classes of fatty acid lipids, glycerophospholipids, hopanoids, sphingolipids and sterol lipids. Moreover, these regions were also characterised by signals at *m/z* 71.989, 811.410 and 825.401 tentatively assigned to be hydroxylamine, a triterpene saponin-like compound and a nucleoside-like compound, respectively. Finally, eight signals (i.e. the *m/z* 1419.956, 1421.856, 1447.818, 1461.858, 1606.755, 1622.825, 1636.829, 1650.838) detected in the CC and OR of AZ78 macrocolonies grown on RMA did not match with any compound in the database so far (Figure 4A; Table A.1).

AZ78 macrocolonies developed on LBA and RMA shared some signals with different distribution according to the growth medium. For instance, signals at *m/z* 96.077 and 112.051 that might match with amine derivatives were found only in the OR of AZ78 macrocolonies on RMA, while they

were present in the CC and OR in the case of AZ78 macrocolonies on LBA. Similarly, the signal at *m/z* 156.042, tentatively assigned to be indole, was found in the CC, OR and GM on LBA, while only in the OR on RMA (Figure 4A, C). The signal at *m/z* 602.919 that might match with a pyrimidine nucleotide sugar was found in CC and OR on RMA and only in GM on LBA (Figure 4A). Other signals were specific for AZ78 macrocolonies developed on LBA, as in the case of the signals at *m/z* 74.097 and 257.149 possibly matching with amine derivatives and a cyclodipeptide respectively found in CC and OR on LBA and the signal at *m/z* 265.966 matching with a pyrrole derivative found in GM on LBA (Figure 4A, D; Table A.2).

The influence of the growth media on the production and release of antibiotics was determined by coupling genome mining and MALDI-TOF-MSI. Firstly, an antiSMASH analysis was carried out to identify genome regions putatively involved in the biosynthesis of secondary metabolites. This analysis revealed the presence of genome regions showing similarity with already known regions involved in the biosynthesis of antibiotics by *L. enzymogenes* strains (Table 2). In particular, the region 1.3 showed 100% of similarity with a genome region of *L. enzymogenes* C3 involved in the biosynthesis of the polycyclic tetramate lactam dihydromalthophilin/HSAF (Figure A3A; Yu et al., 2007) whereas the region 1.1 showed 50% similarity with the genome region of *L. enzymogenes* OH11 involved in the biosynthesis of the cyclic lipodepsipeptide WAP-8294A2 (Figure A3B; Zhang et al., 2011). The region 1.2 and 1.9 showed 18 and 6% similarity respectively with genome regions responsible for the production of pyrrolopyrazines Le- pyrrolopyrazines A, B and C by *L. enzymogenes* OH11 (Li et al., 2017), and macrocyclic depsipeptide Lysobactin by *Lysobacter* sp. ATCC 53042 (Hou et al., 2011). Other regions did not show similarity with any known cluster and included regions putatively responsible for the biosynthesis of bacteriocins (1.4, 1.6), lanthipeptides (1.5, 3.1) and polyketide-like compounds (2.1; Table 2).

Based on antiSMASH analysis outcome, signals at *m/z* values possibly matching with antibiotics synthesised by *L. enzymogenes* strains were searched in the AZ78 metabolic profiles obtained by

MALDI-TOF-MSI analysis. Signals at *m/z* values of 535.495 and 549.437 possibly match these secondary metabolites, especially those belonging to the polycyclic tetramate macrolactams, such as dihydromalthophilin/HSAF, which was exclusively found in the CC and OR regions of AZ78 macrocolonies developed on RMA (Figure 4A, E; Table A.1). Similarly, signals that might match with polyketide-like compounds of the macrolide class were found at *m/z* 740.452, 754.445, 766.433, 780.424, 792.431, 794.455 in these regions of AZ78 macrocolonies grown on RMA (Figure 4A, F; Table A.1). Moreover, these regions on RMA were also characterised by the presence of signals at *m/z* 776.414 and 823.413 possibly matching with cyclic macrolactam compounds (Figure 4A). Looking at the LBA, the signals at *m/z* 1584.749, 1586.877 and 1598.824 were exclusively found in the CC, OR and GM regions of AZ78 macrocolonies originated on this medium and they might match with secondary metabolites belonging to the cyclic lipodepsipeptides such as WAP-8294A2 (Figure 4A, G; Table A.2). By today, no *m/z* value possibly matching with bacteriocins, lanthipeptides, le-pyrrolopyrazines and lysobactin was found in CC, OR and GM regions of AZ78 grown on LBA and RMA (Table 2; Figure 4).

4. Discussion

Having a picture of how AZ78 might behave in the rhizosphere may provide useful insights on its ability to colonise this environment and to produce bioactive secondary metabolites. To take this picture, we formulated an agarised growth medium reproducing the nutrient conditions found in the rhizosphere considering the amount of organic carbon released on average in one day by plants (Jones et al., 2009). The resulting RMA contained root exudates, salts and recalcitrant substances that are found in the rhizosphere, such as cellulose, lignin and starch (Chen et al., 2006). Moreover, we decided to add also humic acids that play an important role in the biotic and abiotic interactions occurring in the rhizosphere (Guo Gao et al., 2015; Kulikova et al., 2016; Olaetxea et al., 2015). We

are aware that RMA is a mere simplification of a natural environment, nonetheless, this medium allowed us to have a glimpse into what AZ78 cells might engage in their natural habitat.

Firstly, the appearance of AZ78 macrocolony on RMA was different compared to that originated on LBA and the main visible differences consisted in the colour and formation of a surrounding halo. In addition, the quantity of AZ78 viable cells present in the macrocolony on RMA was strongly reduced compared to LBA. Since laboratory growth media, as LBA, are richer in nutrients compared to the rhizosphere (Lugtenberg et al., 2017), it was presumable that AZ78 cells might face nutrient limitation during their growth on RMA. Bacteria respond to nutrient limitation through the activity of master regulators, such as the cAMP receptor protein (CRP) firstly described in *Escherichia coli* (Emmer et al., 1970). In this bacterium, CRP is involved in the regulation of carbon metabolism and plays a role in the formation of biofilms and cell surface appendages also (Hardiman et al., 2007; Jackson et al., 2002; Müller et al., 2009; Zheng et al., 2004). Similarly, a cAMP-receptor-like protein (Clp) controls physiological and cellular processes, such as biofilm formation, cell motility and virulence in *Xanthomonas campestris* pv. *campestris* (Chin et al., 2010; He et al., 2007). Interestingly, a *L. enzymogenes* C3 mutant knocked out in *clp* showed different colony morphology compared to the wild type and it was impaired in cell motility (Kobayashi et al., 2005). Moreover, *clp* is crucial in the cell motility and biosynthesis of bioactive secondary metabolites in *L. enzymogenes* OH11 (Qian et al., 2013; Wang et al., 2014). Based on these evidences, we assessed *clp* involvement in the phenotypic changes observed in AZ78 by monitoring its expression, since AZ78 strain is not genetically tractable. The higher expression level of *clp* in AZ78 grown on RMA compared to LBA indicated that changes in AZ78 cell growth rate and macrocolony morphology are possibly associated with a modulation of *clp* expression.

The changes occurring in the AZ78 colony morphology were further explored through microscopy analysis. In the case of AZ78 macrocolony on LBA, cells disposed themselves on the agar surface in a circular colony composed by multi-layers of cells in the centre core and a mono-layer in the

422 outer ring, acquiring morphology similar to other bacterial strains growing on LBA (Su et al.,
423 2012). On this medium rich in protein content, AZ78 macrocolonies were characterised by the
424 presence of many membrane vesicles probably containing proteolytic enzymes as in the case of
425 *Lysobacter* sp. XL1 (Kudryakova et al., 2016). A different scenario was observed on RMA, where
426 such membrane vesicles were not visible and AZ78 macrocolonies were characterised by an
427 extended mono-layer outer ring including AZ78 cells heterogeneously distributed in small groups.
428 TEM observations indicated that the small AZ78 cell groups originated on RMA were embedded in
429 a dense layer of fibrils that may be part of a biofilm (Jones et al., 1969). Accordingly, AZ78 cells
430 produced a biofilm in RM broth and, on RMA; they were equipped by surface appendages that play
431 a key role in biofilm formation and plant root colonisation in *Lysobacter* members (Islam, 2010;
432 Islam et al., 2005; Xia et al., 2018). Biofilms are cosy niches where some bacterial cells may
433 become metabolically less active, reducing the overall growth rate (Guilhen et al., 2016; Wan et al.,
434 2018). Accordingly, we observed that the AZ78 growth was lower on RMA than LBA, where it was
435 also possible to observe AZ78 cells in division. In the process of biofilm dispersal, it is well
436 accepted that individual cells and multicellular aggregates are released from the biofilm to colonise
437 new environments (Guilhen et al., 2017; Hunt et al., 2004). It is conceivable that AZ78 forms a
438 biofilm on RMA that reaches a mature stage after 36 h and cells located in the mono-layer outer
439 ring differentiate into a subpopulation to explore the surrounding areas. Indeed, microscope analysis
440 revealed that the AZ78 cells located in this region were moving whereas they were immobile in the
441 centre core.

442 The AZ78 cell motility may be related to the formation of cell surface appendages, that we
443 previously showed to be dependent on the growth medium composition (Tomada et al., 2016), and
444 to the release of amphipathic compounds (Mattingly et al., 2018). Indeed, many *m/z* signals
445 putatively matching with lipids were found only in RMA and could be involved in the reduction of
446 surface tension to facilitate cell motility and to disperse cells from biofilm (Glick et al., 2010;

Kinsinger et al., 2003; Wang et al., 2013, 2011). Interestingly, a signal at *m/z* 156.042 that might match indole was found in the outer ring of AZ78 grown on RMA. Recently, indole was proven to improve nutrient absorption and regulate twitching motility in *L. enzymogenes* OH11 (Feng et al., 2019; Wang et al., 2019). Therefore, it is conceivable that indole may serve to increase the nutrient uptake in single starved AZ78 cells once they move from the biofilm. Notably, the biofilm formation and the cell dispersal observed on RMA are strategies that AZ78 might implement also in the rhizosphere given the importance to reach nutrients before other competitors as well as to firmly occupy the most favourable ecological niches (Kamilova et al., 2005).

As nutrient conditions affect the production of secondary metabolites in *Lysobacter* spp. (Folman et al., 2004; Lazazzara et al., 2017; Wang et al., 2016), the different AZ78 phenotype on the two growth media was also associated to a substantial difference between the metabolic profiles retrieved from MALDI-TOF-MSI. Particularly, the RMA nutrient conditions increased the diversity of analytes produced by AZ78 compared to LBA. This latter growth medium was characterised by the specific presence of a signal at *m/z* 257.149 matching with a putative cyclodipeptide confirming the ability of AZ78 to produce compounds belonging to this family, such as cyclo-L-Pro-L-Tyr (Puopolo et al., 2014b). Similarly, AZ78 released in LBA an analyte with *m/z* 265.966 that matches pyrrole derivatives, not only confirming the ability of *Lysobacter* spp. to produce pyrrole, but also localising it when grown in protein rich growth media (Lazazzara et al., 2017). The putative cyclic lipodepsipeptides WAP-8294A1/A2/A4 (respectively *m/z* 1586.877, 1584.749, 1598.824) were exclusively detected on LBA, confirming the presence of an AZ78 genome region showing similarity with a homologous region in *L. enzymogenes* OH11 involved in the biosynthesis of cyclic lipodepsipeptides (Zhang et al., 2011). However, the comparison of the two genome regions revealed differences in the arrangement of the regions deputed to the biosynthesis of cyclic lipodepsipeptides indicating that the AZ78 genome region may be involved in the production of novel bioactive metabolites and this would deserve more attention in future studies.

Generally, higher ion intensities were visible in the outer ring of AZ78 macrocolony grown on RMA compared to the centre core. Consistently with previous studies (Yu et al., 2007), the putative dihydromalthophilin/HSAF signal (*m/z* 535.495) was found in nutrient-limited conditions, namely on RMA, and was not detected on LBA. The presence of this substance confirmed the high similarity level found between the AZ78 genome region and the genome region of *L. enzymogenes* C3 deputed to the biosynthesis of the dihydromalthophilin/HSAF (Yu et al., 2007). Another proof of the production of this metabolite relied on the presence of the signal at *m/z* 549.437 that might match with other polycyclic tetramate macrolactams such as alteramide B (*m/z* 549.37 $[M+K]^+$), catacandins A/B (*m/z* 549.37 $[M+K]^+$), and malthophilin (*m/z* 549.39 $[M+K]^+$). Indeed, alteramide B and malthophilin are compounds very close to dihydromalthophilin/HSAF and probably they are intermediate in the synthesis of this compound (Lou et al., 2011). Within the signals exclusively found on RMA, the tentative assigned compounds match with other bioactive secondary metabolites belonging to the family of cyclodepsipeptides (*m/z* 742.397, 748.365), cyclic macrolactams (*m/z* 776.414 and 823.413) and macrolides (*m/z* 740.452, 754.445, 766.433, 780.424, 792.431, 794.455) and it would be interesting to assess the genome region involved in the production of these metabolites in future studies.

Overall, the use of a growth medium mimicking the rhizosphere highlighted how nutrient conditions stimulated processes as cell motility, biofilm formation and biosynthesis of bioactive secondary metabolites in AZ78. All these processes were also associated with a positive modulation of the master regulator *clp*, which role is highly conserved in the members of the *Xanthomonadaceae* family and in *L. enzymogenes* also (Qian et al., 2013; Wang et al., 2014). AZ78 showed physiological traits fundamental to survive in the rhizosphere, such as attachment to surfaces and biofilm formation, as well as quick movement and colonisation of new niches, producing a variety of secondary metabolites to antagonise competitors. However, more work is

needed to characterise AZ78 secondary metabolites and to investigate the role of other components of the microbial community on the physiological traits associated to its rhizosphere competency.

5. Author contributions

F.B. carried out all the experiments, analysed the data, wrote and edited the manuscript. M.M.D. carried out MALDI-TOF-MSI, wrote and edited the manuscript. R.M. carried out TEM analysis, wrote and edited the manuscript. M.P. and I.P. contributed to the conception of the work and edited the manuscript. G.P. conceived the study, designed the experiments, coordinated all research activities and edited the manuscript. All the authors have read the manuscript and agreed to its content.

6. Acknowledgements

We thank Carmela Sicher and Samuele Zoratto for technical assistance. This work was co-funded by the Fondazione Edmund Mach of San Michele all'Adige, Italy, and by the University of Udine, Italy. F.B. was partially supported by the COST Action CA17121 Correlated Multimodal Imaging in Life Sciences (COMULIS).

7. References

Amin, S.A., Hmelo, L.R., van Tol, H.M., Durham, B.P., Carlson, L.T., Heal, K.R., Morales, R.L., Berthiaume, C.T., Parker, M.S., Djunaedi, B., Ingalls, A.E., Parsek, M.R., Moran, M.A., Armbrust, E.V., 2015. Interaction and signalling between a cosmopolitan phytoplankton and associated bacteria. Nature 522, 98–101. https://doi.org/10.1038/nature14488.

Aslam, Z., Yasir, M., Jeon, C.O., Chung, Y.R., 2009. *Lysobacter oryzae* sp. nov., isolated from the rhizosphere of rice (*Oryza sativa* L.). Int. J. Syst. Evol. Micr. 59, 675–680. https://doi.org/10.1099/ijs.0.000588-0.

519 Baudoin, E., Benizri, E., Guckert, A., 2003. Impact of artificial root exudates on the bacterial
520 community structure in bulk soil and maize rhizosphere. Soil Biol. Biochem. 35, 1183–1192.
521 https://doi.org/10.1016/S0038-0717(03)00179-2.

522 Blin, K., Shaw, S., Steinke, K., Villebro, R., Ziemert, N., Lee, S.Y., Medema, M.H., Weber, T.,
523 2019. antiSMASH 5.0: updates to the secondary metabolite genome mining pipeline. Nucleic
524 Acids Res. https://doi.org/10.1093/nar/gkz310.

525 Chen, J., Shen, D., Odhiambo, B.O., Xu, D., Han, S., Chou, S.-H., Qian, G., 2018. Two direct gene
526 targets contribute to Clp-dependent regulation of type IV pilus-mediated twitching motility in
527 *Lysobacter enzymogenes* OH11. Appl. Microbiol. Biot. 102, 7509–7519.
528 https://doi.org/10.1007/s00253-018-9196-x.

529 Chen, M.-C., Wang, M.-K., Chiu, C.-Y., Huang, P.-M., King, H.-B., 2001. Determination of low
530 molecular weight dicarboxylic acids and organic functional groups in rhizosphere and bulk
531 soils of Tsuga and Yushania in a temperate rain forest. Plant Soil 231, 37–44.
532 https://doi.org/10.1023/A:1010347421351.

533 Chen, Y.M., Wang, M.K., Zhuang, S.Y., Chiang, P.N., 2006. Chemical and physical properties of
534 rhizosphere and bulk soils of three tea plants cultivated in Ultisols. Geoderma 136, 378–387.
535 https://doi.org/10.1016/J.GEODERMA.2006.04.003.

536 Chin, K.-H., Lee, Y.-C., Tu, Z.-L., Chen, C.-H., Tseng, Y.-H., Yang, J.-M., Ryan, R.P., McCarthy,
537 Y., Dow, J.M., Wang, A.H.-J., Chou, S.-H., 2010. The cAMP Receptor-Like Protein CLP Is a
538 Novel c-di-GMP Receptor Linking Cell–Cell Signaling to Virulence Gene Expression in
539 *Xanthomonas campestris*. J. Mol. Biol. 396, 646–662.
540 https://doi.org/10.1016/j.jmb.2009.11.076.

541 Cowles, K.N., Gitai, Z., 2010. Surface association and the MreB cytoskeleton regulate pilus
542 production, localization and function in *Pseudomonas aeruginosa*. Mol. Microbiol. 76, 1411–

543 1426. https://doi.org/10.1111/j.1365-2958.2010.07132.x.

544 Debois, D., Fernandez, O., Franzil, L., Jourdan, E., de Brogniez, A., Willems, L., Clément, C.,
545 Dorey, S., De Pauw, E., Ongena, M., 2015. Plant polysaccharides initiate underground
546 crosstalk with bacilli by inducing synthesis of the immunogenic lipopeptide surfactin. Env.
547 Microbiol. Rep. 7, 570–582. https://doi.org/10.1111/1758-2229.12286.

548 Ding, Y., Li, Z., Li, Y., Lu, C., Wang, H., Shen, Y., Du, L., 2016. HSAF-induced antifungal effects
549 in *Candida albicans* through ROS-mediated apoptosis. RSC Adv. 6, 30895–30904.
550 https://doi.org/10.1039/C5RA26092B.

551 Doornbos, R.F., van Loon, L.C., Bakker, P.A.H.M., 2012. Impact of root exudates and plant
552 defense signaling on bacterial communities in the rhizosphere. A review. Agron. Sustain. Dev.
553 32, 227–243. https://doi.org/10.1007/s13593-011-0028-y.

554 Downie, H., Holden, N., Otten, W., Spiers, A.J., Valentine, T.A., Dupuy, L.X., 2012. Transparent
555 soil for imaging the rhizosphere. PLOS ONE 7, e44276.
556 https://doi.org/10.1371/journal.pone.0044276.

557 Emmer, M., deCrombrugghe, B., Pastan, I., Perlman, R., 1970. Cyclic AMP receptor protein of *E.*
558 *coli*: its role in the synthesis of inducible enzymes. P. Natl. Acad. Sci. U.S.A. 66, 480–487.
559 https://doi.org/10.1073/pnas.66.2.480.

560 Feng, T., Han, Y., Li, B., Li, Z., Yu, Y., Sun, Q., Li, X., Du, L., Zhang, X-H., Wang Y., 2019.
561 Interspecies and intraspecies signals synergistically regulate the twitching motility in
562 *Lysobacter enzymogenes*. Appl. Environ. Microb. 8, pii: e01742-19.
563 https://doi.org/10.1128/AEM.01742-19.

564 Folman, L., De Klein, M.J.E., Postma, J., van Veen, J., 2004. Production of antifungal compounds
565 by *Lysobacter enzymogenes* isolate 3.1T8 under different conditions in relation to its efficacy

as a biocontrol agent of *Pythium aphanidermatum* in cucumber. Biol. Control 31, 145–154. https://doi.org/10.1016/j.biocontrol.2004.03.008.

Glick, R., Gilmour, C., Tremblay, J., Satanower, S., Avidan, O., Deziel, E., Greenberg, E.P., Poole, K., Banin, E., 2010. Increase in rhamnolipid synthesis under iron-limiting conditions influences surface motility and biofilm formation in *Pseudomonas aeruginosa*. J. Bacteriol. 192, 2973–2980. https://doi.org/10.1128/JB.01601-09.

Goel, A.K., Rajagopal, L., Nagesh, N., Sonti, R.V., 2002. Genetic locus encoding functions involved in biosynthesis and outer membrane localization of xanthomonadin in *Xanthomonas oryzae* pv. *oryzae*. J. Bacteriol. 184, 3539–3548. https://doi.org/10.1128/jb.184.13.3539-3548.2002.

Grayston, S.J., Wang, S., Campbell, C.D., Edwards, A.C., 1998. Selective influence of plant species on microbial diversity in the rhizosphere. Soil Biol. Biochem. 30, 369–378. https://doi.org/10.1016/S0038-0717(97)00124-7.

Guilhen, C., Charbonnel, N., Parisot, N., Gueguen, N., Iltis, A., Forestier, C., Balestrino, D., 2016. Transcriptional profiling of *Klebsiella pneumoniae* defines signatures for planktonic, sessile and biofilm-dispersed cells. BMC Genomics 17, 237. https://doi.org/10.1186/s12864-016-2557-x.

Guilhen, C., Forestier, C., Balestrino, D., 2017. Biofilm dispersal: multiple elaborate strategies for dissemination of bacteria with unique properties. Mol. Microbiol. 105, 188–210. https://doi.org/10.1111/mmi.13698.

Guo Gao, T., Yuan Xu, Y., Jiang, F., Zhen Li, B., Shui Yang, J., Tao Wang, E., Li Yuan, H., 2015. Nodulation characterization and proteomic profiling of *Bradyrhizobium liaoningense* CCBAU05525 in response to water-soluble humic materials. Sci. Rep. 5, 10836. https://doi.org/10.1038/srep10836.

590 Hardiman, T., Lemuth, K., Keller, M.A., Reuss, M., Siemann-Herzberg, M., 2007. Topology of the
591 global regulatory network of carbon limitation in *Escherichia coli*. J. Biotechnol. 132, 359–
592 374. https://doi.org/10.1016/j.jbiotec.2007.08.029.

593 He, F., Li, B., Ai, G., Kange, A., Zhao, Y., Zhang, X., Jia, Y., Dou, D., Liu, F., Cao, H., 2018.
594 Transcriptomics analysis of the chinese pear pathotype of *Alternaria alternata* gives insights
595 into novel mechanisms of HSAF antifungal activities. Int. J. Mol. Sci. 19, 1841.
596 https://doi.org/10.3390/ijms19071841.

597 He, Y.-W., Ng, A.Y.-J., Xu, M., Lin, K., Wang, L.-H., Dong, Y.-H., Zhang, L.-H., 2007.
598 *Xanthomonas campestris* cell-cell communication involves a putative nucleotide receptor
599 protein Clp and a hierarchical signalling network. Mol. Microbiol. 64, 281–292.
600 https://doi.org/10.1111/j.1365-2958.2007.05670.x.

601 Hellemans, J., Mortier, G., De Paepe, A., Speleman, F., Vandesompele, J., 2007. qBase relative
602 quantification framework and software for management and automated analysis of real-time
603 quantitative PCR data. Genome Biol. 8, R19. https://doi.org/10.1186/gb-2007-8-2-r19.

604 Holzlechner, M., Reitschmidt, S., Gruber, S., Zeilinger, S., Marchetti-Deschmann, M., 2016.
605 Visualizing fungal metabolites during mycoparasitic interaction by MALDI mass spectrometry
606 imaging. Proteomics 16, 1742–1746. https://doi.org/10.1002/pmic.201500510.

607 Hou, J., Robbel, L., Marahiel, M.A., 2011. Identification and characterization of the Lysobactin
608 biosynthetic gene cluster reveals mechanistic insights into an unusual termination module
609 architecture. Chem. Biol. 18, 655–664. https://doi.org/10.1016/j.chembiol.2011.02.012.

610 Hunt, S.M., Werner, E.M., Huang, B., Hamilton, M.A., Stewart, P.S., 2004. Hypothesis for the role
611 of nutrient starvation in biofilm detachment. Appl. Environ. Microb. 70, 7418–7425.
612 https://doi.org/10.1128/AEM.70.12.7418-7425.2004.

613 Islam, M.T., 2010. Mode of antagonism of a biocontrol bacterium *Lysobacter* sp. SB-K88 toward a
614 damping-off pathogen *Aphanomyces cochlioides*. World J. Microb. Biot. 26, 629–637.
615 https://doi.org/10.1007/s11274-009-0216-y.

616 Islam, M.T., Hashidoko, Y., Deora, A., Ito, T., Tahara, S., 2005. Suppression of damping-off
617 disease in host plants by the rhizoplane bacterium *Lysobacter* sp. strain SB-K88 is linked to
618 plant colonization and antibiosis against soilborne Peronosporomycetes. Appl. Environ.
619 Microb. 71, 3786–3796. https://doi.org/10.1128/AEM.71.7.3786-3796.2005.

620 Jackson, D.W., Simecka, J.W., Romeo, T., 2002. Catabolite repression of *Escherichia coli* biofilm
621 formation. J. Bacteriol. 184, 3406–3410. https://doi.org/10.1128/jb.184.12.3406-3410.2002.

622 Jones, D.L., Nguyen, C., Finlay, R.D., 2009. Carbon flow in the rhizosphere: carbon trading at the
623 soil-root interface. Plant Soil 321, 5–33. https://doi.org/10.1007/s11104-009-9925-0.

624 Jones, H.C., Roth, I.L., Sanders, W.M., 1969. Electron microscopic study of a slime layer. J.
625 Bacteriol. 99, 316–25.

626 Kamilova, F., Kravchenko, L. V., Shaposhnikov, A.I., Azarova, T., Makarova, N., Lugtenberg, B.,
627 2006. Organic acids, sugars, and L-tryptophane in exudates of vegetables growing on
628 stonewool and their effects on activities of rhizosphere bacteria. Mol. Plant Microbe In. 19,
629 250–256. https://doi.org/10.1094/MPMI-19-0250.

630 Kamilova, F., Validov, S., Azarova, T., Mulders, I., Lugtenberg, B., 2005. Enrichment for enhanced
631 competitive plant root tip colonizers selects for a new class of biocontrol bacteria. Environ.
632 Microbiol. 7, 1809–1817. https://doi.org/10.1111/j.1462-2920.2005.00889.x.

633 Kim, S.-J., Ahn, J.-H., Weon, H.-Y., Joa, J.-H., Hong, S.-B., Seok, S.-J., Kim, J.-S., Kwon, S.-W.,
634 2017. *Lysobacter solanacearum* sp. nov., isolated from rhizosphere of tomato. Int. J. Syst.
635 Evol. Micr. 67, 1102–1106. https://doi.org/10.1099/ijsem.0.001729.

636 Kinsinger, R.F., Shirk, M.C., Fall, R., 2003. Rapid surface motility in *Bacillus subtilis* is dependent
637 on extracellular surfactin and potassium ion. J. Bacteriol. 185, 5627–5631.
638 https://doi.org/10.1128/jb.185.18.5627-5631.2003.

639 Klinkert, I., Chughtai, K., Ellis, S.R., Heeren, R.M.A., 2014. Methods for full resolution data
640 exploration and visualization for large 2D and 3D mass spectrometry imaging datasets. Int. J.
641 Mass Spectrom. 362, 40–47. https://doi.org/10.1016/J.IJMS.2013.12.012.

642 Kobayashi, D.Y., Reedy, R.M., Palumbo, J.D., Zhou, J.-M., Yuen, G.Y., 2005. A *clp* gene
643 homologue belonging to the Crp gene family globally regulates lytic enzyme production,
644 antimicrobial activity, and biological control activity expressed by *Lysobacter enzymogenes*
645 strain C3. Appl. Environ. Microb. 71, 261–269. https://doi.org/10.1128/AEM.71.1.261-
646 269.2005.

647 Kobayashi, Y., Lakshmanan, V., Kobayashi, Y., Asai, M., Iuchi, S., Kobayashi, M., Bais, H.P.,
648 Koyama, H., 2013. Overexpression of AtALMT1 in the *Arabidopsis thaliana* ecotype
649 Columbia results in enhanced Al-activated malate excretion and beneficial bacterium
650 recruitment. Plant Signal. Behav. 8, e25565. https://doi.org/10.4161/psb.25565.

651 Kudryakova, I. V., Shishkova, N.A., Vasilyeva, N. V., 2016. Outer membrane vesicles of
652 *Lysobacter* sp. XL1: biogenesis, functions, and applied prospects. Appl. Microbiol. Biot. 100,
653 4791–4801. https://doi.org/10.1007/s00253-016-7524-6.

654 Kulikova, N.A., Abroskin, D.P., Badun, G.A., Chernysheva, M.G., Korobkov, V.I., Beer, A.S.,
655 Tsvetkova, E.A., Senik, S. V, Klein, O.I., Perminova, I. V, 2016. Label distribution in tissues
656 of wheat seedlings cultivated with tritium-labeled Leonardite humic acid. Sci. Rep. 6, 28869.
657 https://doi.org/10.1038/srep28869.

658 Lazazzara, V., Perazzolli, M., Pertot, I., Biasioli, F., Puopolo, G., Cappellin, L., 2017. Growth
659 media affect the volatilome and antimicrobial activity against *Phytophthora infestans* in four

660 *Lysobacter* type strains. Microbiol. Res. 201, 52–62.
661 https://doi.org/10.1016/J.MICRES.2017.04.015.

662 Li, S., Calvo, A.M., Yuen, G.Y., Du, L., Harris, S.D., 2009. Induction of cell wall thickening by the
663 antifungal compound dihydromaltophilin disrupts fungal growth and is mediated by
664 sphingolipid biosynthesis. J. Eukaryot. Microbiol. 56, 182–187. https://doi.org/10.1111/j.1550-
665 7408.2008.00384.x.

666 Li, S., Jochum, C.C., Yu, F., Zaleta-Rivera, K., Du, L., Harris, S.D., Yuen, G.Y., 2008. An
667 antibiotic complex from *Lysobacter enzymogenes* strain C3: antimicrobial activity and role in
668 plant disease control. Phytopathology 98, 695–701. https://doi.org/10.1094/PHYTO-98-6-
669 0695.

670 Li, S., Wu, X., Zhang, L., Shen, Y., Du, L., 2017. Activation of a cryptic gene cluster in *Lysobacter*
671 *enzymogenes* reveals a module/domain portable mechanism of nonribosomal peptide
672 synthetases in the biosynthesis of pyrrolopyrazines. Org. Lett. 19, 5010–5013.
673 https://doi.org/10.1021/acs.orglett.7b01611.

674 Lou, L., Qian, G., Xie, Y., Hang, J., Chen, H., Zaleta-Rivera, K., Li, Y., Shen, Y., Dussault, P.H.,
675 Liu, F., Du, L., 2011. Biosynthesis of HSAF, a tetramic acid-containing macrolactam from
676 *Lysobacter enzymogenes*. J. Am. Chem. Soc. 133, 643–645. https://doi.org/10.1021/ja105732c.

677 Lugtenberg, B., Rozen, D.E., Kamilova, F., 2017. Wars between microbes on roots and fruits.
678 F1000Res. 6, 343. https://doi.org/10.12688/F1000RESEARCH.10696.1.

679 Lynch, J.M., Whipps, J.M., 1990. Substrate flow in the rhizosphere. Plant Soil 129, 1–10.
680 https://doi.org/10.1007/BF00011685.

681 Mattingly, A.E., Weaver, A.A., Dimkovikj, A., Shrout, J.D., 2018. Assessing travel conditions:
682 environmental and host influences on bacterial surface motility. J. Bacteriol. 200, e00014-18.

683 https://doi.org/ 10.1128/JB.00014-18.

684 Müller, C.M., Åberg, A., Straseviçiene, J., Emődy, L., Uhlin, B.E., Balsalobre, C., 2009. Type 1
685 fimbriae, a colonization factor of uropathogenic *Escherichia coli*, are controlled by the
686 metabolic sensor CRP-cAMP. PLOS Pathog. 5, e1000303.
687 https://doi.org/10.1371/journal.ppat.1000303.

688 Nakayama, T., Homma, Y., Hashidoko, Y., Mizutani, J., Tahara, S., 1999. Possible role of
689 xanthobaccins produced by *Stenotrophomonas* sp. strain SB-K88 in suppression of sugar beet
690 damping-off disease. Appl. Environ. Microb. 65, 4334–43339.

691 Nihorimbere, V., Cawoy, H., Seyer, A., Brunelle, A., Thonart, P., Ongena, M., 2012. Impact of
692 rhizosphere factors on cyclic lipopeptide signature from the plant beneficial strain *Bacillus*
693 *amyloliquefaciens* S499. FEMS Microbiol. Ecol. 79, 176–191. https://doi.org/10.1111/j.1574-
694 6941.2011.01208.x.

695 Olaetxea, M., Mora, V., Bacaicoa, E., Baigorri, R., Garnica, M., Fuentes, M., Casanova, E.,
696 Zamarreño, A.M., Iriarte, J.C., Etayo, D., Ederra, I., Gonzalo, R., Garcia-Mina, J.M., 2015.
697 ABA-regulation of root hydraulic conductivity and aquaporin gene- expression is crucial to the
698 plant shoot rise caused by rhizosphere humic acids. Plant Physiol. 169, 2587–2596.
699 https://doi.org/10.1104/pp.15.00596.

700 Park, J.H., Kim, R., Aslam, Z., Jeon, C.O., Chung, Y.R., 2008. *Lysobacter capsici* sp. nov., with
701 antimicrobial activity, isolated from the rhizosphere of pepper, and emended description of the
702 genus *Lysobacter*. Int. J. Syst. Evol. Micr. 58, 387–392. https://doi.org/10.1099/ijs.0.65290-0.

703 Pfeifer, B.A., Khosla, C., 2001. Biosynthesis of polyketides in heterologous hosts. Microbiol. Mol.
704 Biol. R. 65, 106–118. https://doi.org/10.1128/MMBR.65.1.106-118.2001.

705 Postma, J., Scheper, R.W.A., Schilder, M.T., 2010. Effect of successive cauliflower plantings and

706 *Rhizoctonia solani* AG 2-1 inoculations on disease suppressiveness of a suppressive and a
707 conducive soil. Soil Biol. Biochem. 42, 804–812.
708 https://doi.org/10.1016/J.SOILBIO.2010.01.017.

709 Puopolo, G., Cimmino, A., Palmieri, M.C., Giovannini, O., Evidente, A., Pertot, I., 2014b.
710 *Lysobacter capsici* AZ78 produces cyclo(L-Pro-L-Tyr), a 2,5-diketopiperazine with toxic
711 activity against sporangia of *Phytophthora infestans* and *Plasmopara viticola*. J. Appl.
712 Microbiol. 117, 1168–1180. https://doi.org/10.1111/jam.12611.

713 Puopolo, G., Giovannini, O., Pertot, I., 2014a. *Lysobacter capsici* AZ78 can be combined with
714 copper to effectively control *Plasmopara viticola* on grapevine. Microbiol. Res. 169, 633–642.
715 https://doi.org/10.1016/j.micres.2013.09.013.

716 Puopolo, G., Tomada, S., Pertot, I., 2018. The impact of the omics era on the knowledge and use of
717 *Lysobacter* species to control phytopathogenic micro-organisms. J. Appl. Microbiol. 124, 15–
718 27. https://doi.org/10.1111/jam.13607.

719 Puopolo, G., Tomada, S., Sonego, P., Moretto, M., Engelen, K., Perazzolli, M., Pertot, I., 2016. The
720 *Lysobacter capsici* AZ78 genome has a gene pool enabling it to interact successfully with
721 phytopathogenic microorganisms and environmental factors. Front. Microbiol. 7, 96.
722 https://doi.org/10.3389/fmicb.2016.00096.

723 Qian, G., Wang, Y., Liu, Y., Xu, F., He, Y.-W., Du, L., Venturi, V., Fan, J., Hu, B., Liu, F., 2013.
724 *Lysobacter enzymogenes* uses two distinct cell-cell signaling systems for differential regulation
725 of secondary-metabolite biosynthesis and colony morphology. Appl. Environ. Microb. 79,
726 6604–6616. https://doi.org/10.1128/AEM.01841-13.

727 Robichaud, G., Garrard, K.P., Barry, J.A., Muddiman, D.C., 2013. MSiReader: an open-source
728 interface to view and analyze high resolving power MS imaging files on Matlab platform. J.
729 Am. Soc. Mass Spectr. 24, 718–721. https://doi.org/10.1007/s13361-013-0607-z.

730 Rodrigues, R.R., Rodgers, N.C., Wu, X., Williams, M.A., 2018. COREMIC: a web-tool to search
731 for a niche associated CORE MICrobiome. PeerJ 6, e4395. https://doi.org/10.7717/peerj.4395.

732 Rosenzweig, N., Tiedje, J.M., Quensen, J.F., Meng, Q., Hao, J.J., 2012. Microbial communities
733 associated with potato common scab-suppressive soil determined by pyrosequencing analyses.
734 Plant Dis. 96, 718–725. https://doi.org/10.1094/PDIS-07-11-0571.

735 Ruijter, J.M., Ramakers, C., Hoogaars, W.M.H., Karlen, Y., Bakker, O., van den Hoff, M.J.B.,
736 Moorman, A.F.M., 2009. Amplification efficiency: linking baseline and bias in the analysis of
737 quantitative PCR data. Nucleic Acids Res. 37, e45. https://doi.org/10.1093/nar/gkp045.

738 Schneider, C.A., Rasband, W.S., Eliceiri, K.W., 2012. NIH Image to ImageJ: 25 years of image
739 analysis. Nat. Methods 9, 671–675. https://doi.org/10.1038/nmeth.2089.

740 Seccareccia, I., Kost, C., Nett, M., 2015. Quantitative analysis of *Lysobacter* predation. Appl.
741 Environ. Microb. 81, 7098–7105. https://doi.org/10.1128/AEM.01781-15.

742 Su, P.-T., Liao, C.-T., Roan, J.-R., Wang, S.-H., Chiou, A., Syu, W.-J., 2012. Bacterial colony from
743 two-dimensional division to three-dimensional development. PLOS ONE 7, e48098.
744 https://doi.org/10.1371/journal.pone.0048098.

745 Tomada, S., Puopolo, G., Perazzolli, M., Musetti, R., Loi, N., Pertot, I., 2016. Pea broth enhances
746 the biocontrol efficacy of *Lysobacter capsici* AZ78 by triggering cell motility associated with
747 biogenesis of type IV pilus. Front. Microbiol. 7, 1136.
748 https://doi.org/10.3389/fmicb.2016.01136.

749 Uren, N., 2007. Types, amounts, and possible functions of compounds released into the rhizosphere
750 by soil-grown plants. In: Pinton, R., Varanini, Z., Nannipieri, P. (Eds.), The Rhizosphere. CRC
751 Press, Boca Raton, pp. 1-21. https://doi.org/10.1201/9781420005585.

752 van Hees, P.A.W., Jones, D.L., Finlay, R., Godbold, D.L., Lundström, U.S., 2005. The carbon we

753 do not see-the impact of low molecular weight compounds on carbon dynamics and respiration
754 in forest soils: a review. Soil Biol. Biochem. 37, 1–13.
755 https://doi.org/10.1016/J.SOILBIO.2004.06.010.

756 Villa-Rodríguez, E., Ibarra-Gámez, C., de los Santos-Villalobos, S., 2018. Extraction of high-
757 quality RNA from *Bacillus subtilis* with a lysozyme pre-treatment followed by the Trizol
758 method. J. Microbiol. Meth. 147, 14–16. https://doi.org/10.1016/J.MIMET.2018.02.011.

759 Villadsen, N.L., Jacobsen, K.M., Keiding, U.B., Weibel, E.T., Christiansen, B., Vosegaard, T.,
760 Bjerring, M., Jensen, F., Johannsen, M., Tørring, T., Poulsen, T.B., 2017. Synthesis of ent-BE-
761 43547A1 reveals a potent hypoxia-selective anticancer agent and uncovers the biosynthetic
762 origin of the APD-CLD natural products. Nat. Chem. 9, 264–272.
763 https://doi.org/10.1038/nchem.2657.

764 Walker, T.S., Bais, H.P., Grotewold, E., Vivanco, J.M., 2003. Root exudation and rhizosphere
765 biology. Plant Physiol. 132, 44–51. https://doi.org/10.1104/pp.102.019661.

766 Wan, N., Wang, H., Ng, C.K., Mukherjee, M., Ren, D., Cao, B., Tang, Y.J., 2018. Bacterial
767 metabolism during biofilm growth investigated by 13C tracing. Front. Microbiol. 9, 2657.
768 https://doi.org/10.3389/fmicb.2018.02657.

769 Wang, J., Yu, B., Tian, D., Ni, M., 2013. Rhamnolipid but not motility is associated with the
770 initiation of biofilm seeding dispersal of *Pseudomonas aeruginosa* strain PA17. J. Biosciences
771 38, 149–156. https://doi.org/10.1007/s12038-012-9297-0.

772 Wang, R., Khan, B.A., Cheung, G.Y.C., Bach, T.-H.L., Jameson-Lee, M., Kong, K.-F., Queck,
773 S.Y., Otto, M., 2011. *Staphylococcus epidermidis* surfactant peptides promote biofilm
774 maturation and dissemination of biofilm-associated infection in mice. J. Clin. Invest. 121, 238–
775 248. https://doi.org/10.1172/JCI42520.

776 Wang, R., Xu, H., Du, L., Chou, S.-H., Liu, H., Liu, Y., Liu, F., Qian, G., 2016. A TonB-dependent
777 receptor regulates antifungal HSAF biosynthesis in *Lysobacter*. Sci. Rep. 6, 26881.
778 https://doi.org/10.1038/srep26881.

779 Wang, R., Zhang, H., Sun, L., Qi, G., Chen, S., Zhao, X., 2017. Microbial community composition
780 is related to soil biological and chemical properties and bacterial wilt outbreak. Sci. Rep. 7,
781 343. https://doi.org/10.1038/s41598-017-00472-6.

782 Wang, Y., Tian, T., Zhang, J., Jin, X., Yue, H., Zhang, X.-H., Du, L., Bai, F., 2019. Indole reverses
783 intrinsic antibiotic resistance by activating a novel dual-function importer. MBio 10, e00676-
784 19. https://doi.org/10.1128/mBio.00676-19.

785 Wang, Y., Zhao, Yuxin, Zhang, J., Zhao, Yangyang, Shen, Y., Su, Z., Xu, G., Du, L., Huffman,
786 J.M., Venturi, V., Qian, G., Liu, F., 2014. Transcriptomic analysis reveals new regulatory roles
787 of Clp signaling in secondary metabolite biosynthesis and surface motility in *Lysobacter*
788 *enzymogenes* OH11. Appl. Microbiol. Biot. 98, 9009–9020. https://doi.org/10.1007/s00253-
789 014-6072-1.

790 Xia, J., Chen, J., Chen, Y., Qian, G., Liu, F., 2018. Type IV pilus biogenesis genes and their roles in
791 biofilm formation in the biological control agent *Lysobacter enzymogenes* OH11. Appl.
792 Microbiol. Biot. 102, 833–846. https://doi.org/10.1007/s00253-017-8619-4.

793 Xie, Y., Wright, S., Shen, Y., Du, L., 2012. Bioactive natural products from *Lysobacter*. Nat. Prod.
794 Rep. 29, 1277. https://doi.org/10.1039/c2np20064c.

795 Xu, L., Wu, P., Wright, S.J., Du, L., Wei, X., 2015. Bioactive polycyclic tetramate macrolactams
796 from *Lysobacter enzymogenes* and their absolute configurations by theoretical ECD
797 calculations. J. Nat. Prod. 78, 1841–1847. https://doi.org/10.1021/acs.jnatprod.5b00099.

798 Yang, J., Caprioli, R.M., 2011. Matrix sublimation/recrystallization for imaging proteins by mass

spectrometry at high spatial resolution. Anal. Chem. 83, 5728–5734. https://doi.org/10.1021/ac200998a.

Yu, F., Zaleta-Rivera, K., Zhu, X., Huffman, J., Millet, J.C., Harris, S.D., Yuen, G., Li, X.-C., Du, L., 2007. Structure and biosynthesis of Heat-Stable Antifungal Factor (HSAF), a broad-spectrum antimycotic with a novel mode of action. Antimicrob. Agents Ch. 51, 64–72. https://doi.org/10.1128/AAC.00931-06.

Yuen, G.Y., Broderick, K.C., Jochum, C.C., Chen, C.J., Caswell-Chen, E.P., 2018. Control of cyst nematodes by *Lysobacter enzymogenes* strain C3 and the role of the antibiotic HSAF in the biological control activity. Biol. Control 117, 158–163. https://doi.org/10.1016/J.BIOCONTROL.2017.11.007.

Zhalnina, K., Louie, K.B., Hao, Z., Mansoori, N., da Rocha, U.N., Shi, S., Cho, H., Karaoz, U., Loqué, D., Bowen, B.P., Firestone, M.K., Northen, T.R., Brodie, E.L., 2018. Dynamic root exudate chemistry and microbial substrate preferences drive patterns in rhizosphere microbial community assembly. Nat. Microbiol. 3, 470–480. https://doi.org/10.1038/s41564-018-0129-3.

Zhang, W., Li, Y., Qian, G., Wang, Y., Chen, H., Li, Y.-Z., Liu, F., Shen, Y., Du, L., 2011. Identification and characterization of the anti-methicillin-resistant *Staphylococcus aureus* WAP-8294A2 biosynthetic gene cluster from *Lysobacter enzymogenes* OH11. Antimicrob. Agents Ch. 55, 5581–5589. https://doi.org/10.1128/AAC.05370-11.

Zheng, D., Constantinidou, C., Hobman, J.L., Minchin, S.D., 2004. Identification of the CRP regulon using *in vitro* and *in vivo* transcriptional profiling. Nucleic Acids Res. 32, 5874–5893. https://doi.org/10.1093/nar/gkh908.

8. Web References

antiSMASH Bacterial Version. https://antismash.secondarymetabolites.org/ (accessed 2019).

822 The Metabolomics Workbench. http://www.metabolomicsworkbench.org/ (accessed 2019).

823 The R Project for Statistical Computing. https://www.r-project.org/ (accessed 2019).

824 **Figure captions**

825 **Figure 1. *Lysobacter capsici* AZ78 macrocolony morphology and growth on the two growth**
826 **media**. AZ78 cell suspension was spot inoculated on Luria–Bertani Agar (LBA; A) and
827 Rhizosphere-Mimicking Agar (RMA; B) and incubated at 25°C for 36 h. The arrow indicates a halo
828 surrounding AZ78 macrocolony (B). The viable cells of AZ78 were monitored at 12, 24, 36 hours
829 post-inoculation on LBA and RMA (C). A Two-way ANOVA revealed no significant differences
830 between two independent experiments (P = 0.43) and data were pooled. The mean cell
831 concentration ± standard error values of 18 replicates (Petri dishes) from two experiments are
832 reported. For each time point, asterisk indicate values that differ significantly according to Student's
833 t-test ($\alpha = 0.05$).
834
835 **Figure 2. Visualization of the growth front of *Lysobacter capsici* AZ78 macrocolony.** AZ78 cell
836 suspension was spot inoculated on a thin layer of on Luria–Bertani Agar (A, B) or Rhizosphere-
837 Mimicking Agar (C, D) on glass slides and incubated at 25°C for 36 h. AZ78 was observed with a
838 phase-contrast microscope at magnification 20× (A, C) and 100× (B, D). The white bar corresponds
839 to 1 mm and the black bar corresponds to 10 μm.
840
841 **Figure 3. Visualization of *Lysobacter capsici* AZ78 cellular morphology**. AZ78 cell suspensions
842 were spot inoculated on Luria–Bertani Agar (LBA; A, B, C) and Rhizosphere-Mimicking Agar
843 (RMA; D, E, F) dishes and incubated at 25°C for 36 h and analysed by transmission electron
844 microscopy. On LBA nucleoid-like less electron-dense areas in the cytoplasm (n), long fibrils (lf),
845 membrane vesicles (v) and cellular detritus (d) were visible. On RMA, fibrils (f), electron-dense

granules (g), polar fimbriae (pf) were visible. The white bar corresponds to 1 μm, the black bar corresponds to 500 nm.

Figure 4. Mass spectrometric imaging of *Lysobacter capsici* AZ78 grown in the two growth media. Some signals of interest identified in the MALDI-TOF-MSI analysis were selected and reported in the presence/absence analysis (A). AZ78 macrocolony was divided in three regions of interest: the centre core of the macrocolony (CC), the outer ring of the macrocolony (OR), and the growth medium adjacent to the outer ring (GM) (B). Grey colour indicates the presence of the ion in the corresponding region of interest (A). The optical images of the AZ78 macrocolony grown on Luria–Bertani Agar (LBA; left) and Rhizosphere-Mimicking Agar (RMA; right) were acquired just before matrix application. MALDI-TOF-MSI images were recorded at a lateral resolution of 150 x 75 μm and represent TIC (total ion count) normalised data corresponding to *m/z* 156.042, 257.149, 535.495, 740.452 and 1584.749 ± 0.1 Th (respectively C, D, E, F, G), the colour bar shows the intensity values.

Figure A1. Expression analysis of *clp* in *Lysobacter capsici* AZ78 grown in the two media. The normalised relative quantity (NRQ) for the *clp* expression in AZ78 grown on Luria–Bertani Agar (LBA) and Rhizosphere-Mimicking Agar (RMA) at 25°C for 36 h was calculated. A two-way ANOVA revealed no significant difference between two independent experiments ($P = 0.27$) and data were pooled. Columns represent mean NRQ ± standard errors of three replicates for each treatment. Asterisk indicates values that differ significantly according to Student's t-test ($\alpha = 0.05$).

Figure A2. Biofilm formation by *Lysobacter capsici* AZ78 grown in the two liquid media. The specific biofilm formation (SBF) values were calculated for AZ78 grown in and Luria–Bertani broth (LB) and Rhizosphere-Mimicking broth (RM). A two-way ANOVA revealed no significant difference between two independent experiments ($P = 0.24$) and data were pooled. Columns

represent mean specific biofilm formation ± standard errors of ten replicates. Asterisk indicates values that differ significantly according to Student's t-test ($\alpha = 0.05$).

Figure A3. Dihydromalthophilin and WAP-8294A gene organization in the *Lysobacter capsici* AZ78, *L. enzymogenes* C3 and *L. enzymogenes* OH11 genome. Putative genes encoding dihydromalthophilin/HSAF in the AZ78 genome are compared to the homologue putative genes in the *L. enzymogenes* C3 (A). Putative genes encoding involved in the biosynthesis of the cyclic lipodepsipeptide WAP-8294A in the AZ78 genome are compared to the homologue putative genes in the *L. enzymogenes* OH11 genome (B). The corresponding accession number is given under each gene.

Animation A1. Movement of *Lysobacter capsici* AZ78 cells on growth media. AZ78 cell suspensions were spot inoculated on a thin layer of Luria–Bertani Agar (LBA; A) or Rhizosphere-Mimicking Agar (RMA; B) on glass slides and incubated at 25°C for 36 h. Ten subsequent pictures were taken each ten seconds and reproduced with an interval of 0.5 s.

891 **Table 1. Composition of Rhizosphere Mimicking Agar.**

Type	Ingredients[a]	Concentration (g/l)
Synthetic root exudates	Citric acid	0.8838
	Fructose[b]	3.3149
	Glucose	3.3223
	Glutamic acid	1.6184
	L-Alanine	1.6393
	L-Serine	1.9337
	Lactic acid	0.8287
	Succinic acid	1.1337
	Sucrose	3.1491
Recalcitrant organic carbon sources	Cellulose	0.0787
	Humic acids	0.0330
	Lignin	0.0650
	Starch	0.0167
Salts	$CuSO_4$ $5H_2O$	0.0030
	KCl	0.4995
	KH_2PO_4	0.6804
	$Fe_2(SO_4)_3$	0.0031
	$MgSO_4$ $7H_2O$	0.4929
	$MnSO_4$	0.0004
	Na_2MoO_4 $2H_2O$	0.0034
	$(NH_4)_2SO_4$	0.0010

892 [a]The pH was adjusted to 6.5 and agar was added in a concentration of 1.6 % (w/v)

893 [b]Fructose, glucose and sucrose were added after autoclaving

894

895

Table 2. Regions of *Lysobacter capsici* AZ78 genome potentially involved in the biosynthesis of bioactive secondary metabolites.

Region[a]	From (bp)	To (bp)	Type[b]	Potential product[c]	Similar cluster[d]	Similarity[e]	*m/z*[f]	Reference
1.1[g]	460,280	648,277	NRPS, Type I PKS	Cyclic depsipeptide	WAP-8294A2	50%	1562.83	Zhang et al. (2011)
1.2	1,093,882	1,113,823	Lanthipeptide cluster	Lanthipeptide	Le-pyrrolopyrazines	18%	193.13	Li et al. (2017)
1.3	1,347,924	1,397,412	Type I PKS, NRPS	Polycyclic tetramate lactam	Dihydromalthophilin/HSAF	100%	513.30	Yu et al. (2007)
1.4	1,468,724	1,478,439	Bacteriocin	Bacteriocin	Unknown	_	_	_
1.5	2,928,156	2,928,156	Lanthipeptide cluster	Lanthipeptide	Unknown	_	_	_
1.6	3,764,006	3,764,006	Bacteriocin	Bacteriocin	Unknown	_	_	_
1.7	4,143,953	4,185,179	Aryl polyene cluster	Arylpolyene	Xanthomonadin	57%	552.00	Goel et al. (2002)
1.8	4,245,240	4,329,436	NRPS	Cyclic depsipeptide	BE-43547 A1-C2	13%	_	Villadsen et al. (2017)
1.9	4,447,365	4,470,235	Lanthipeptide cluster	Lanthipeptide	Lysobactin	6%	1276.73	Hou et al. (2011)
2.1	182,279	223,271	PKS-like	Polyketide-like	Unknown	_	_	_
3.1	4,629	27,295	Lanthipeptide cluster	Lanthipeptide	Unknown	_	_	_

[a]Regions of *Lysobacter capsici* AZ78 genome (JAJA02000000.2) identified through antiSMASH 5.0.0 analysis using default settings and extra features such as KnownClusterBlast, ClusterBlast, ActiveSiteFinder, Cluster Pfam analysis and Pfam-based GO term annotation.

[b]Class of genes cluster according to antiSMASH 5.0.0

[c]Family of probable syntethised bioactive metabolites based on the region of *L. capsici* AZ78 genome

[d]Most similar cluster based on antiSMASH 5.0.0 analysis

[e]Percentage of similar genes located in closest similar cluster

[f]Mass-to-charge ratios $[M+H]^+$

[g]Regions 1.1-1.9, 2.1 and 3.1 are respectively located in the contigs JAJA02000001.1, JAJA02000002.1 and JAJA02000003.1

Table A.1. Identification of biologically relevant analytes produced by *Lysobacter capsici* AZ78 cells grown on the Rhizosphere Mimicking Agar (RMA) using Matrix Assisted Laser Desorption/Ionisation Time of Flight Mass Spectrometric Imaging (MALDI-TOF-MSI).

Analyte[a]	*m/z*[b]	Possible matching compounds[c]
1	71.989	Hydroxylamine
2	96.077	Amine-derivative
3	112.051	Aniline derivative/Cytosine/Aminopyrimidine/Triazine derivative/Amine derivative
4	156.042	Phosphoethanolamine derivative/Indole derivative/Valine/Betaine/Amino fatty acids
5	498.973	Thiamine pyrophosphate
6	523.455	Fatty acyl lipid
7	535.495	Polycyclic tetramate macrolactams (Dihydromalthophilin/Xanthobaccin B)
8	549.437	Polycyclic tetramate macrolactams (Malthophilin/Alteramide B/Catacandins A/B)
9	602.920	Pyrimidine nucleotide sugar
10	740.452	Macrolide-like antibiotic/Glycerophospholipid
11	742.397	Macrolide-like antibiotic/Cyclodepsipeptide-like antibiotic/Glycerophospholipid
12	748.365	Cyclodepsipeptide-like antibiotic/Sterol lipid/Glycerophospholipid
13	750.467	Glycerophospholipid
14	754.446	Tetracyclic macrolide-like insecticide/Glycerophospholipid
15	762.459	Glycerophospholipid
16	764.433	Glycerophospholipid
17	766.433	Macrolide-like antibiotic/Glycerophospholipid
18	776.414	Cyclic macrolactam/Glycerophospholipid
19	778.430	Glycerophospholipid
20	780.424	Macrolide-like antibiotic/Glycerophospholipid
21	792.431	Macrolide-like antibiotic/Glycerophospholipid
22	794.455	Macrolide-like antibiotic/Glycerophospholipid
23	806.470	Glycerophospholipid
24	811.470	Glycerophospholipid
25	823.413	Cyclic macrolactam/Glycerophospholipid/Sterol lipid
26	825.401	Nucleoside-like antibiotic/Sterol lipid/Glycerophospholipid
27	1,419.956	Unknown
28	1,421.856	Sphingolipid
29	1,423.823	Sphingolipid
30	1,447.818	Unknown
31	1,461.859	Unknown
32	1,606.755	Unknown
33	1,622.825	Unknown
34	1,636.829	Unknown
35	1,650.838	Unknown

[a]Analytes produced by *L. capsici* AZ78 cells identified through MALDI-TOF-MSI using a Synapt G2 HDMS system

[b]Mass-to-charge ratios $[M+H]^+$

[c]All *m/z* values were searched in "Metabolomics Workbench" metabolite database (https://www.metabolomicsworkbench.org/, 2019) to tentatively assign a matching compound.

Table A.2. Identification of biologically relevant analytes produced by *Lysobacter capsici* AZ78 cells grown on the Luria-Bertani Agar (LBA) using Matrix Assisted Laser Desorption/Ionisation Time of Flight Mass Spectrometric Imaging (MALDI-TOF-MSI).

Analyte[a]	*m/z*[b]	Possible matching compounds[c]
1	74.097	Amine derivative
2	96.077	Amine-derivative
3	112.051	Aniline derivative/Cytosine/Aminopyrimidine/Triazine derivative/Amine derivative
4	156.042	Phosphoethanolamine derivative/Indole derivative/Valine/Betaine/Amino fatty acids
5	257.149	Cyclodipeptide
6	265.966	Pyrrole derivative/Benzoyl derivative
7	602.920	Pyrimidine nucleotide sugar
8	1,584.749	Cyclic lipodepsipeptide (WAP-8294A2)
9	1,586.877	Cyclic lipodepsipeptide (WAP-8294A1)
10	1,598.824	Cyclic lipodepsipeptide (WAP-8294A4)

[a]Analytes produced by *L. capsici* AZ78 cells identified through MALDI-TOF-MSI using a Synapt G2 HDMS system

[b]Mass-to-charge ratios $[M+H]^+$

[c]All *m/z* values were searched in "Metabolomics Workbench" metabolite database (https://www.metabolomicsworkbench.org/, 2019) to tentatively assign a matching compound.

925

926 **Animation A1A**

Animation A1A_031219.mp4

927

928

929

930 **Animation A1B**

Animation A1B_031219.mp4

931

Figure 1

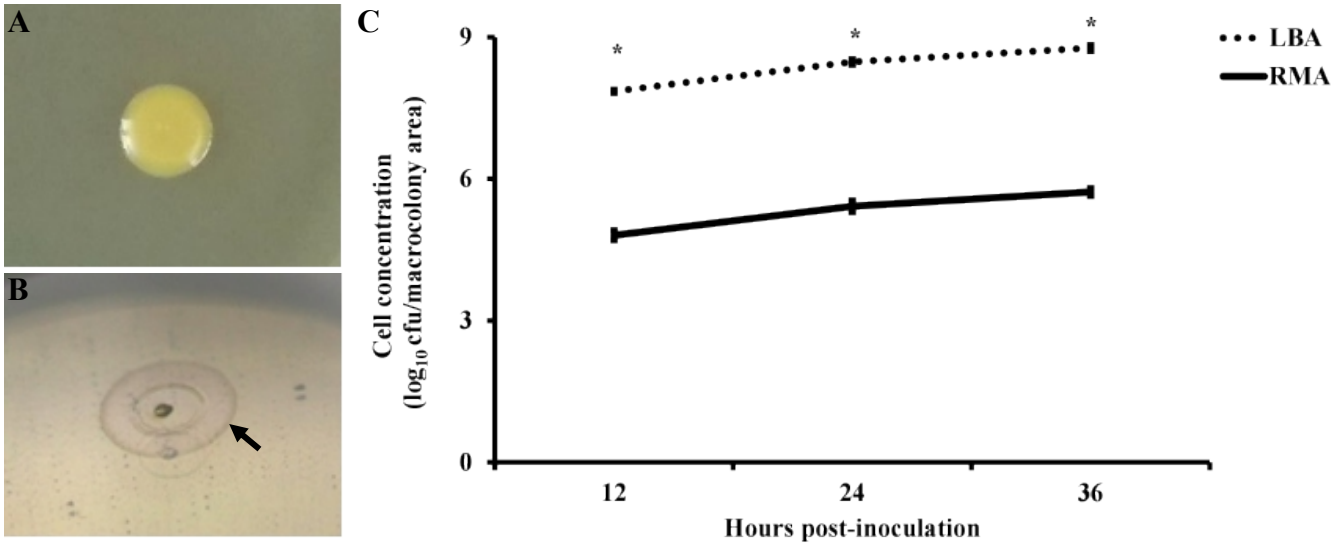
A
B
C
9
6
3
0
12
24
36
Hours post-inoculation
Cell concentration
(log10 cfu/macrocolony area)
LBA
RMA
*
*
*

Figure 2

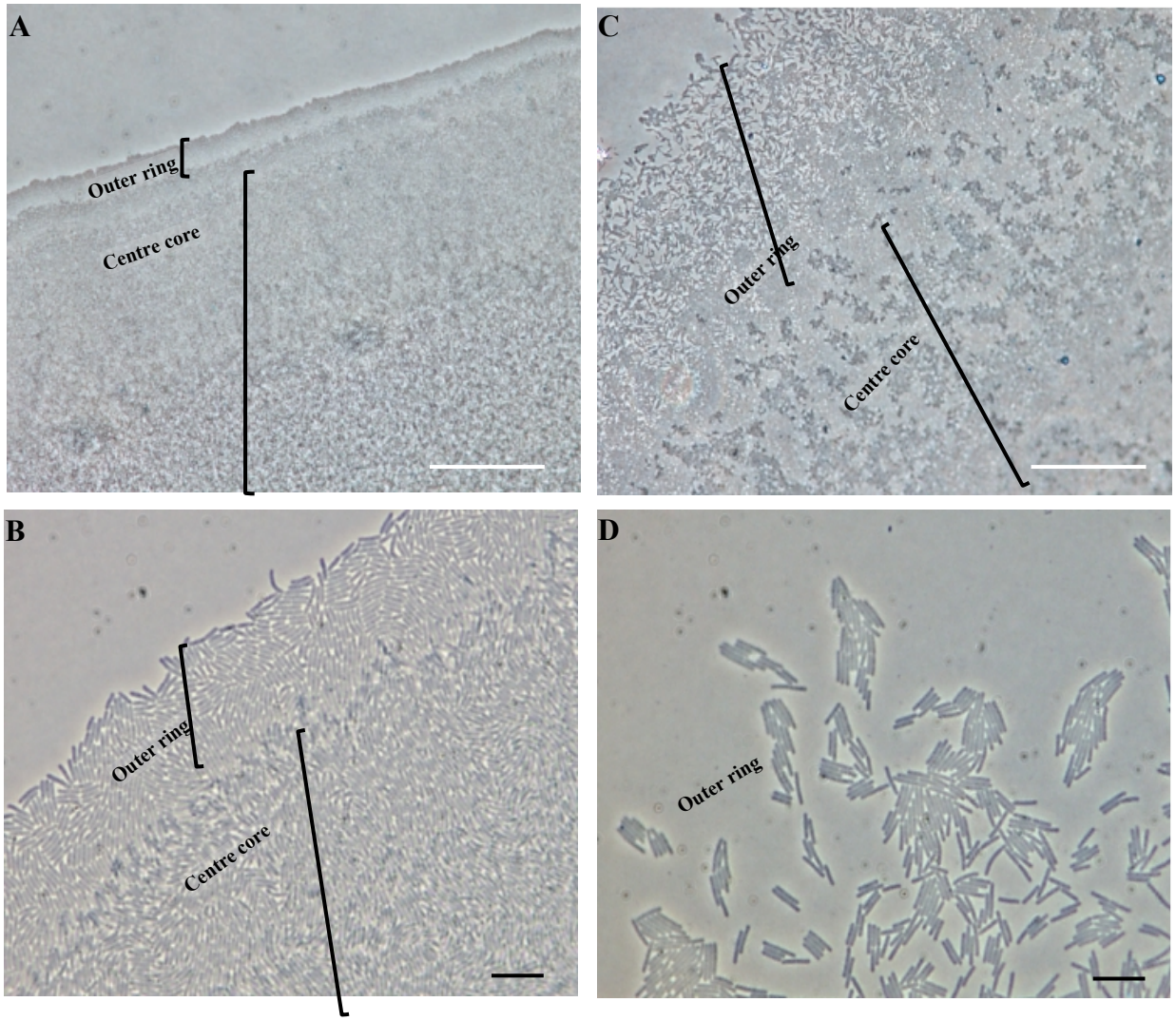
A
Outer ring
Centre core
C
Outer ring
Centre core
B
Outer ring
Centre core
D
Outer ring

Figure 3

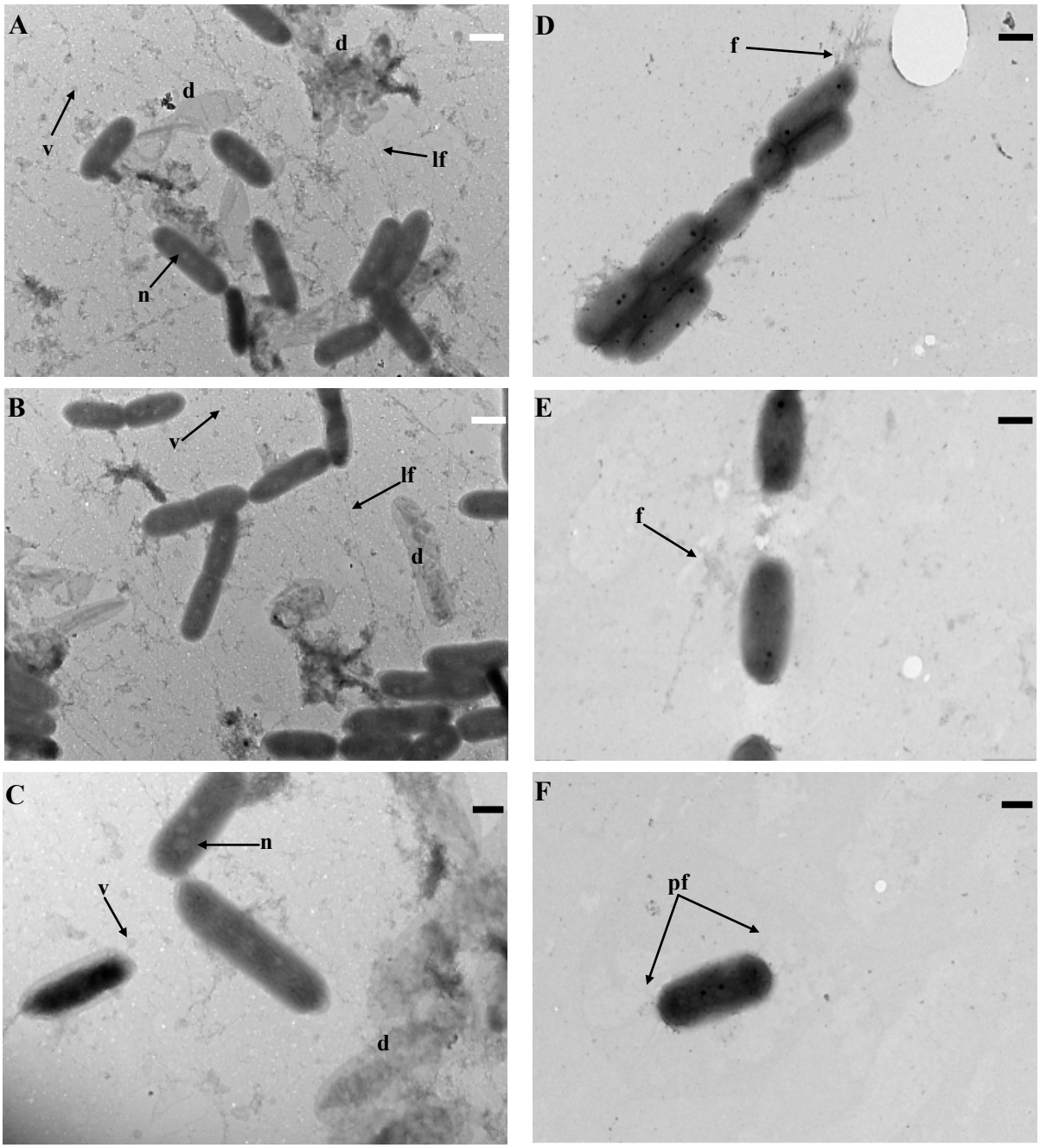

Figure 4

A

m/z	LBA			RMA		
	CC	OR	GM	CC	OR	GM
71.989				■	■	
74.097	■	■				
96.077	■	■			■	
112.051	■	■			■	
156.042	■	■	■		■	
257.149	■	■				
265.966			■			
498.973					■	
523.455				■	■	
535.495				■	■	
549.437				■	■	
602.920			■	■	■	
740.452				■	■	
742.397				■	■	
748.365				■	■	
750.467				■	■	
754.446				■	■	
762.459				■	■	
764.433				■	■	
766.433				■	■	
776.414				■	■	
778.430				■	■	
780.424				■	■	
792.431				■	■	
794.455				■	■	
806.470				■	■	
811.470				■	■	
823.413				■	■	
825.401				■	■	
1,419.956				■	■	
1,421.856				■	■	
1,423.823				■	■	
1,447.818				■	■	
1,461.859				■	■	
1,584.749	■	■	■			
1,586.877	■	■	■			
1,598.824	■	■	■			
1,606.755				■	■	
1,622.825				■	■	
1,636.829				■	■	
1,650.838				■	■	

B

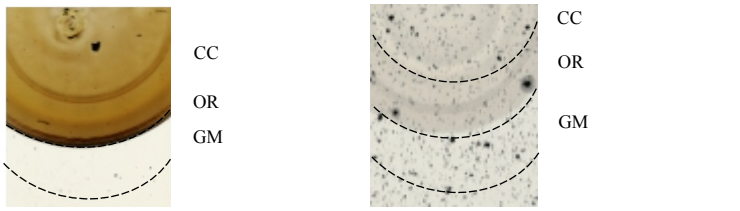

C *m/z* 156.042

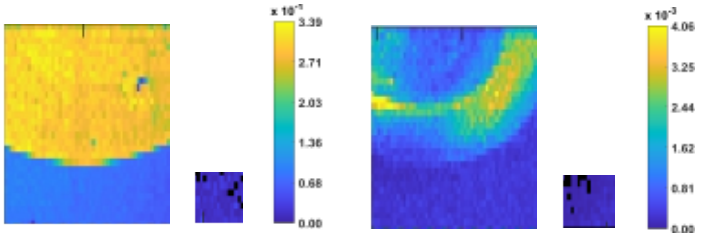

D *m/z* 257.149

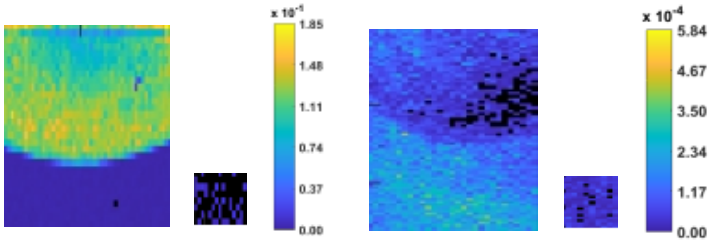

E *m/z* 535.495

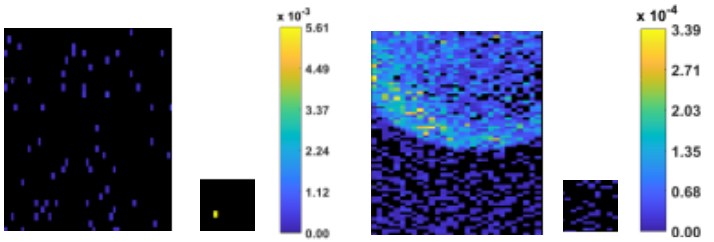

F *m/z* 740.452

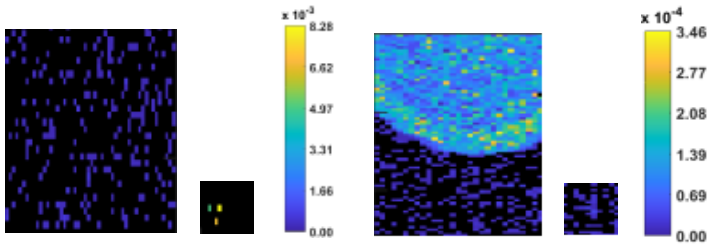

G *m/z* 1584.749

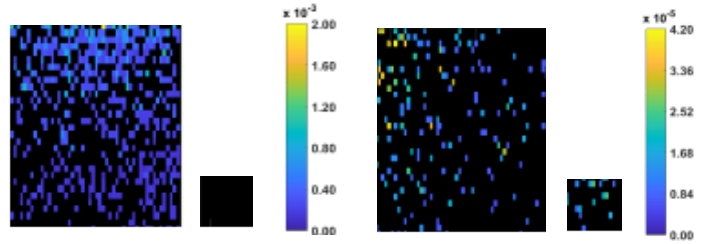

AZ78 on LBA LBA AZ78 on RMA RMA

Figure A1

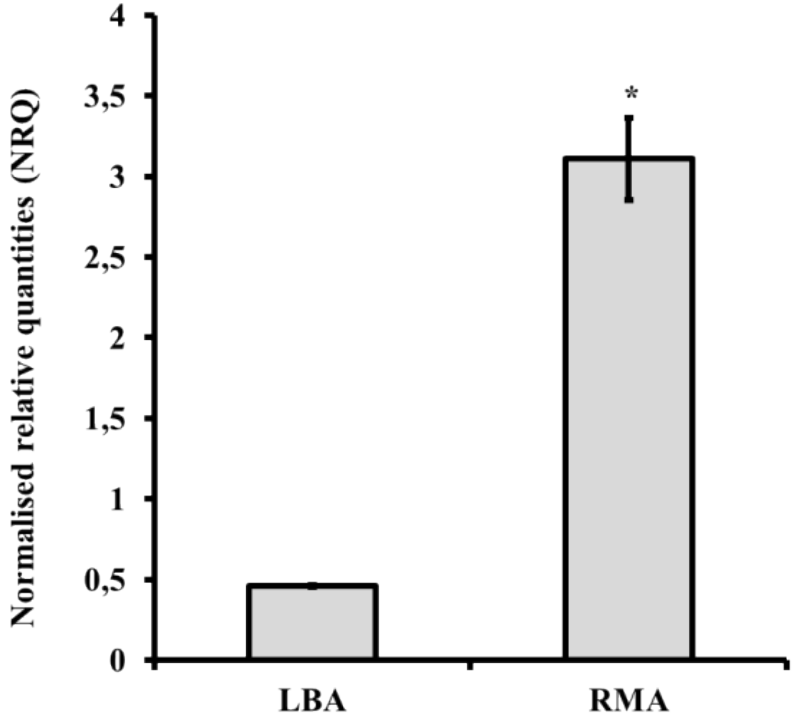
Normalised relative quantities (NRQ)
4
3,5
3
2,5
2
1,5
1
0,5
0
*
LBA
RMA

Figure A2

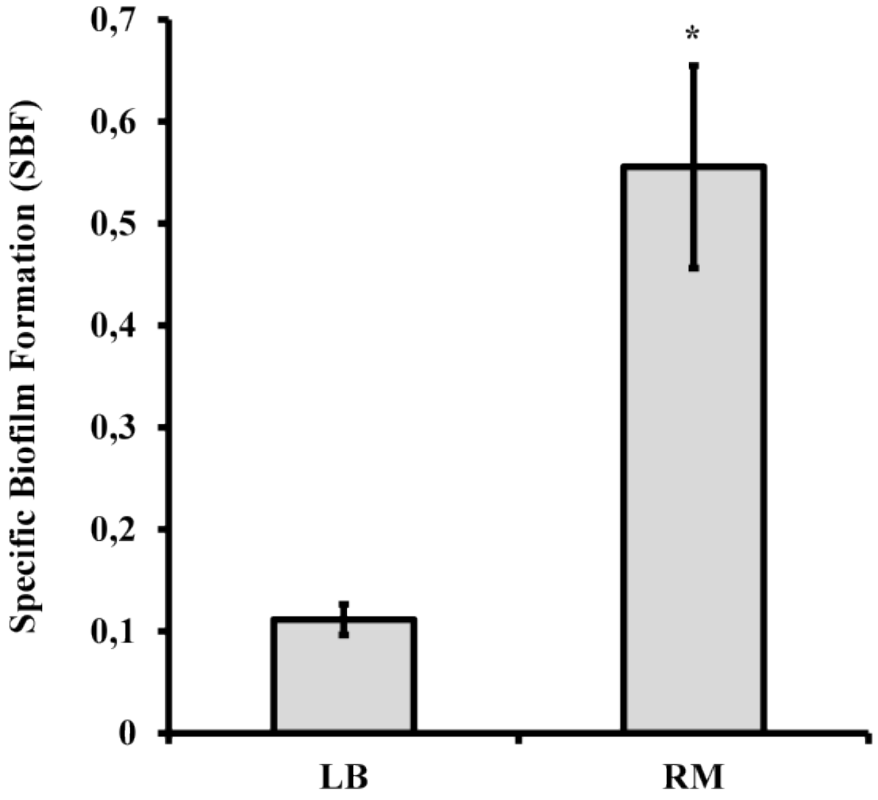

Figure A3

A

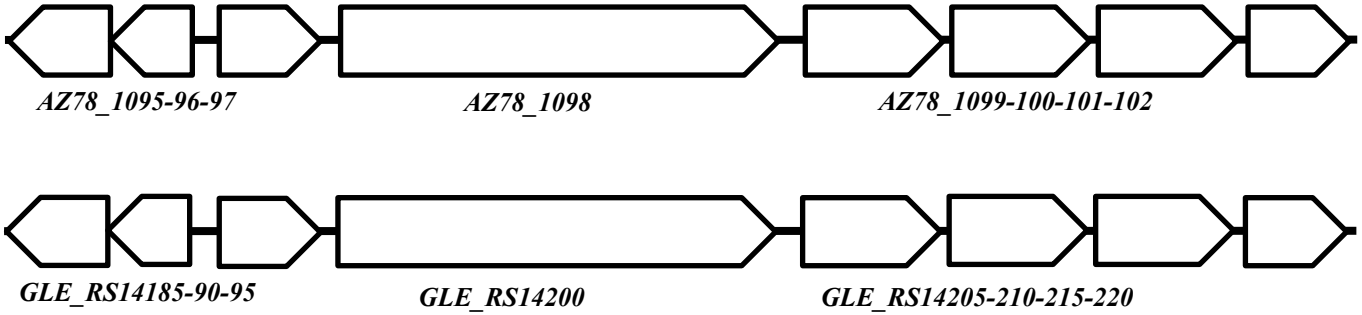
AZ78_1095-96-97
AZ78_1098
AZ78_1099-100-101-102
GLE_RS14185-90-95
GLE_RS14200
GLE_RS14205-210-215-220

B

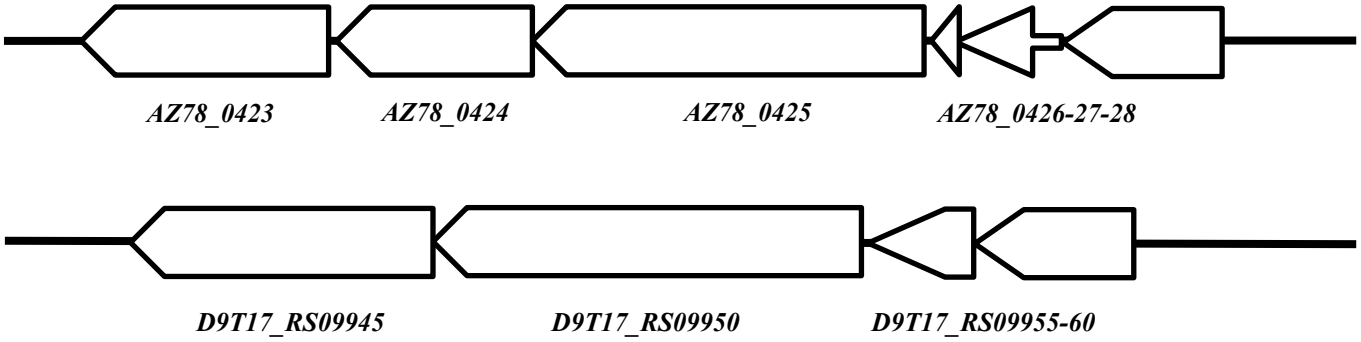
AZ78_0423
AZ78_0424
AZ78_0425
AZ78_0426-27-28
D9T17_RS09945
D9T17_RS09950
D9T17_RS09955-60

Declaration of interests

 The authors declare that they have no known competing financial interests or personal relationships that could have appeared to influence the work reported in this paper.

☐The authors declare the following financial interests/personal relationships which may be considered as potential competing interests: